IMPLEMENTING *IN VITRO* SCREENING TOOLS FOR EVALUATION NOVEL MRNA-NANOPARTICULATE FORMULATIONS

by

Toriana Nichole Vigil

A thesis submitted to Johns Hopkins University in conformity with the requirements for the degree of Master of Science in Engineering

Baltimore, Maryland

December 2019

Abstract

3D spheroids of immortalized cell lines and primary human cells were utilized to examine the structure-function relationship of lipid nanoparticles (LNPs). Establishing a rigorous procedure for HepG2 and Hep3b spheroids included determination of appropriate seeding densities and media conditions for LNP transfection. Experimentation with standard and non-standard LNP formulations highlighted significant variation with cell and culture type, thus suggesting that choosing appropriately is of the utmost importance. Furthermore, it was noted that LNP performance should be determined via evaluation in multiple metrics since potency and maximum expression results did not always align. An *in vitro to in vivo* correlation with LNP transfection is ongoing.

Advisors: Dr. Jordan J. Green (JHU), Dr. J. Luis Santos (AstraZeneca), Dr. G. Patrick Hussmann (AstraZeneca)

Additional Readers: Dr. Stavroula Sofou

Acknowledgements

Thank you to the INBT Coop Program for connecting me with this opportunity at AstraZeneca. Many thanks to my mentors Dr. Luis Santos, Dr. Patrick Hussmann, and Dr. Jordan Green for their guidance and expertise in this project. Much appreciation to my colleagues Nicholas Lamb, Dr. Randall Meyer, and Michael Newton for the discussions, troubleshooting, and experimental design help.

Table of Contents

List of Tables

List of Figures

Introduction

Nucleic acids are a promising therapeutic for the treatment of many diseases via modified gene expression and subsequent protein production [1–3]. These results can be achieved via the introduction of a variety of nucleic acids, such as mRNA, siRNA, and anti-sense oligonucleotides. An mRNA-based therapy allows gene expression to occur relatively quickly, in as few as 4-6 hours after dosing because mRNA can be translated to a protein product without entering the nucleus [1,4]. However, in order for these therapies to be effective, sensitive nucleic acid cargoes must be delivered undamaged to their target site, necessitating a drug delivery method that fully shields the cargo from degradation following therapeutic administration and biodistribution. Lipid nanoparticles (LNPs) fully encapsulate their cargo molecules until uptake occurs in target cells; providing mRNA-cargo protection from degradation and shielding from potential immune response [1–3]. Lipid components within LNPs can be varied to control particle size, particle stability, cargo encapsulation, and endosomal escape [2,5–7]. After intravascular administration, LNPs are extracted from plasma via first-pass metabolism in the liver. By nature of their lipid composition, LNPs are then bound by serum-derived Apolipoprotein E and targeted to low density lipoprotein receptors on the hepatocellular surface, thus triggering internalization and delivery [2].

As with most biopharmaceutical candidates, LNPs are often tested *in vitro* prior to introduction in *in vivo* models. Screening of biopharmaceutical candidates *in vitro* is most commonly conducted with immortalized cell lines cultured in 2D monolayers. This practice is well-established, inexpensive, high-throughput, and often a prerequisite to further experiments *in*

vivo. However, identifying successful biopharmaceutical candidates with this screening methodology hinges on a correlation between *in vitro* and *in vivo* results. Immortalized cell lines have characteristic mutations that allow them to be replicated and grown indefinitely *in vitro*, however, these mutations also naturally distinguish them from their counterparts in live tissues. Recent studies highlight the lack of significant correlation between *in vitro* and *in vivo* results, suggesting that current screening standards may be insufficient or misleading, and often resulting in inappropriate identification of lead hits [8,9]. With consideration to the structure and function relationship of lipid components in LNPs, Kulkarni *et al.* show that for delivery of pDNA an unsaturated fatty acid as a helper lipid performs better than a saturated fatty acid *in vitro*, however, the opposite is seen *in vivo* (i.e. a saturated fatty acid helper lipid has superior performance than an unsaturated fatty acid). Similar paradoxical results have been observed when varying other lipid components of LNPs [10,11]. These contradictory results *in vitro* and *in vivo* are just one example of the lack of an *in vitro to in vivo* correlation (IVIVC), and thus inefficiency in current biopharmaceutical screening standards.

This lack of an IVIVC is likely due to the dissimilarities observed for immortalized cell lines in 2D culture as compared to their originating tissues [8]. In 2D culture, immortalized cell lines exhibit limited cell-to-cell interactions and migration, as well as differential adhesion, polarity, and morphologies [12]. These dissimilarities can be overcome by in vitro testing in primary cells [13,14], but this is often very costly, resource intensive, and highly variable. 3D spheroid cultures of immortalized cell lines exhibit intercellular signaling, transport, morphological, and biochemical similarities to tissues in vivo and may offer a promising alternative [15–17]. Furthermore, 3D spheroids have been recognized as an especially useful model in oncology

due to their different layers of proliferation and hypoxic core [17,18]. These characteristics suggest that screening with 3D spheroids may offer more accurate predictive results of biopharmaceutical candidates than screening in 2D culture, while remaining relatively inexpensive and high-throughput.

Through examining the **structure-function relationship of LNPs in 2D and 3D cell culture and *in vivo* models,** we hypothesize that **LNP-mRNA transfections in 3D cultures are more predictive of *in vivo* transfection.** Since LNPs exhibit preferential innate targeting for delivery to the liver [2], *in vitro* experiments include immortalized hepatocellular cell lines HepG2 and Hep3b, and primary human hepatocytes.

Examining an IVIVC has the potential to significantly decrease research and development timelines and costs for new therapeutics [3]. This benefits patients by making cutting-edge therapeutic options available sooner at lower prices. Furthermore, an IVIVC correlation has the potential to decrease the need for animal testing in drug development research, thus further decreasing time, cost, and animal lives needed for developing new therapeutics.

Materials and Methods

Additional information and/or examples can be found in the Supplementary Information.

Cell Growth and Handling

HepG2 and Hep3b 2D Cell Culture: Media for HepG2 was prepared via the combination of 500 mL DMEM, 50 mL FBS, and 5 mL 100x MEM NEAA. This solution was mixed well and filtered to remove any particulates. Media for Hep3b was prepared with 50 mL MEM + GlutaMax, 50 mL FBS, 5 mL NEAA, and 5 mL sodium pyruvate. This solution was mixed well and filtered to remove any particulates. Cells were plated in Corning 96-well tissue-treated flat-bottom plates at seeding densities of 60,000 cells/well in 100 µL total volume with their respective media. Plates were placed in an incubator (37±2 °C, 5±1% CO_2, ≥85% RH) for 24 hours to allow cells to attach. 24 hours after cell seeding plates were transfected with LNPs.

HepG2 and Hep3b 3D Cell Culture: Media for HepG2 and Hep3b cells was prepared as described above. Cells were plated in Corning 96-well ultra-low attachment u-bottom plates at seeding densities of 3,000 cells/well in 100 µL total volume with their respective media.

Primary Human Hepatocytes 2D Cell Culture: Primary human hepatocytes and plating media components were obtained from both Corning and ThermoFisher as available. The plating media was prepared by the combination of 500 mL Williams E, 5 mL Corning ITS Supplements, 5 µL 10 mM dexamethasone, 7.5 mL HEPES, 5 mL Penn/Strep/Glut, and 50 mL FBS. Cells were thawed and dispersed in plating media. Cells were then counted with a Vi-Cell and plated in ThermoFisher 96-well tissue-treated flat-bottom plates at densities of 20,000 cells/well. Plates

were placed in an incubator (37±2 °C, 5±1% CO_2, ≥85% RH) for 24 hours to allow cells to attach. 24 hours after cell seeding plates were transfected with LNPs.

Primary Human Hepatocytes 3D Cell Culture: Primary human hepatocytes and plating media components were obtained from both Corning and ThermoFisher as available. Cells were then prepared according to manufacturer's instructions [19], with some adaptations. Plating media was prepared as described above. Cell maintenance media was also prepared at this time by combining 500 mL Williams E, 5 mL Corning ITS Supplements, 5 µL 10 mM dexamethasone, 7.5 mL HEPES, and 5 mL Penn/Strep/Glut. Both the plating and maintenance media were filtered to remove any particulates.

Cells were thawed and dispersed in plating media. Cells were then counted with a Vi-Cell and plated in ThermoFisher 96-well U-bottom Nunclon Sphera plates at densities of 2,000 cells/well in a total volume of 100 µL. Plates were centrifuged at 100xg for 2 minutes to facilitate early aggregation. Plates were placed in an incubator (37±2 °C, 5±1% CO_2, ≥85% RH) for 48 hours.

After 48 hours, and additional 100 µL of maintenance media was added to each well. Plates were centrifuged at 100xg for 2 minutes and returned to incubator.

96 hours after initial cell seeding 100 µL of media was removed from each well and replaced with 100 µL of fresh maintenance media. Approximately 168 hours after cell seeding plates were transfected with LNPs.

Lipid Nanoparticle Formulation

Lipid nanoparticles were prepared via the combination of two solutions in a microfluidic device. The volumetric ratio of solutions during the mixing process was 1:3 organic to aqueous. Organic solutions (Cholesterol, PEG-DMG, helper lipid, ionizable lipid) were prepared via the suspension of lipid components in ethanol and thorough mixing. Aqueous solutions (RNA-se free water, Citrate Buffer, and mRNA) were prepared with sterile technique in Biological Safety Cabinet. Lipid and mRNA solutions were then loaded in independent syringes and LNP formulations were prepared using a NanoAssemblr mixing device from Precision Nanosystems (PNI, Canada). LNP formulations were collected and analyzed for their size, charge, polydispersity, mRNA percentage encapsulation efficiency, and mRNA content.

A table with additional details concerning LNP formulation and characterization details can be found in the Supplementary Information.

Lipid Nanoparticle Characterization

Ribogreen Assay: Performed a 2% dilution by combining naked mRNA with Tris-EDTA buffer. A standard curve for mRNA luminescence was built in a 96-well plate. Aliquots of the standard curve were divided amongst four columns of wells, where additional Tris-EDTA buffer or Triton X were added for a total volume of 200 µL.

To determine the mRNA content and mRNA encapsulation efficiency, LNPs were then diluted to 2% via combination with Tris-EDTA buffer and mixed well. 50 µL of each LNP dilution was added to four wells, with Tris-EDTA or Triton X buffer added. The Ribogreen solution was

prepared by performing a 5% dilution in Tris-EDTA buffer and mixing well. 100 µL of Ribogreen working solution was added to each well (mRNA standards and LNP samples), mixed well, and inspected for bubbles.

Fluorescence reading was evaluated via a microplate reader with excitation at 495 nm and emission at 525 nm. The standard curve values were then plotted for extrapolation of mRNA sample concentrations.

RP-HPLC: Following LNP concentration calculations, HPLC samples were prepared at 30 µg/mL (based on mRNA) in Tris-EDTA, with 50% total volume Triton X added. Hybrid LNP samples were prepared similarly, except substituting 8mM SDS buffer for Tris-EDTA. Samples were ran in sequence to monitor potential mRNA degradation in relation to an mRNA standard.

Malvern Zeta-sizer: To determine the average size of mRNA encapsulated LNPs, a 0.4% dilution of LNP particles in PBS was performed and gently mixed. A 70 µL sample was transferred to a quartz cuvette for data collection. Through calculations considering the diffusion and Brownian motion of particles, size measurement was calculated via a Stokes-Einstein relationship.

To determine the zeta potential of mRNA encapsulated LNPs, a 0.1% dilution of LNP particles in 10mM NaCL NaP detergent solution. The sample was loaded into a disposable zeta potential cuvette for measurement via Laser Doppler Micro-electrophoresis.

Lipid Nanoparticle Transfection

LNPs were warmed to room temperature and mixed by gentle pipetting with filtered pipette tips. LNPs were diluted to appropriate concentrations (10 µg working mRNA / mL for 2D cultures, 40 µg working mRNA / mL for 3D cultures). For transfection in 2D cultures, a high concentration of 500 ng final mRNA per well with six subsequent two-fold dilutions was prepared. For transfection in 3D cultures, a high concentration of 2000 ng final mRNA per well with nine subsequent two-fold dilutions was prepared.

For 2D plates, 50 µL of each LNP dilution was added to appropriate wells. Then an appropriate volume of media to transfection and blank wells was added for a total volume of 200 µL.

For 3D plates, 50 µL of media was removed from transfection wells, this amount was replaced with 50 µL appropriate LNP dilution solutions.

All plates were returned to incubator (37±2 °C, 5±1% CO_2, ≥85% RH). A Steady-Glo assay to measure luminescence signal resulting from mRNA transcription and Luciferase protein production resulting from successful transfection was performed 24 hours after transfection. Prior to Steady-Glo assay, plates were removed from incubator to equilibrate to room temperature and imaged with Incucyte.

Steady-Glo assay was performed according to manufacturer's instructions, with a shaking period of 20 minutes, and brief monitoring under the microscope to ensure cells are sufficiently detached or disrupted.

For luminescence reading, 100 µL from each well was transferred to white-walled plates and read via Perkin Elmer Envision.

Results and Discussion

I. Development of 3D Spheroid Growth Protocols

Previous literature on the development of 3D spheroid models characterizes cells in one of four categories: single cell suspensions, loose aggregates, compact aggregates, and spheroids (**Figure 1**) [13,20–22]. It is also well-known that spheroids consist of three different inner layers: the proliferative zone, the quiescent zone, and the necrotic core. These zones arise in part due to limited oxygen and nutrient diffusivity through layers of cells, thus defining the cells' metabolic state [16,23]. At this time, there is no defined standard cell seeding density to optimize the balance between necrotic core size in relation to overall spheroid morphology for *in vitro* studies [21], and optimal seeding densities are likely cell line and media dependent. For these reasons, while developing our 3D spheroid growth protocols, we examined different media conditions and seeding densities.

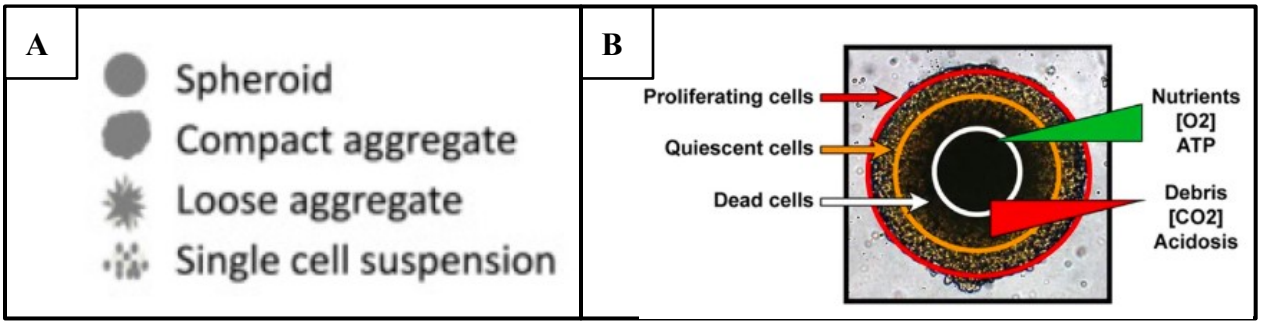

Figure 1. Understanding spheroid morphology classification and different metabolic layers of activity. Panel A from reference 20, *Exp Cell Res.* 2018, 365, 57-65. Panel B from reference 23, *Sci Rep* 2016, 6, 19103.

a. Immortalized Hepatocellular Cell Line: HepG2s

Many researchers seed HepG2 spheroid culture in media containing fetal bovine serum (FBS), then transition to serum-free media to eliminate potential particulates and sources of variability to encourage consistently compact spheroids [13,21,23,24]. Others suggest that when human-derived cell lines, including such as HepG2 cells, are cultured in human serum (HS), they tend to form tighter, more compact spheroids than when cultured in FBS [20] with improved cell functionality and better metabolism of lipids [25]. Increased metabolism of lipids may result in increased transfection efficiency. The HS condition in these studies also included a variety of supplements, in order to more closely resemble cellular contact with interstitial fluid [20]. In order to determine which conditions yielded the best spheroids, we examined different spheroid seeding densities, serum versus serum-free conditions, and culturing in FBS compared to HS.

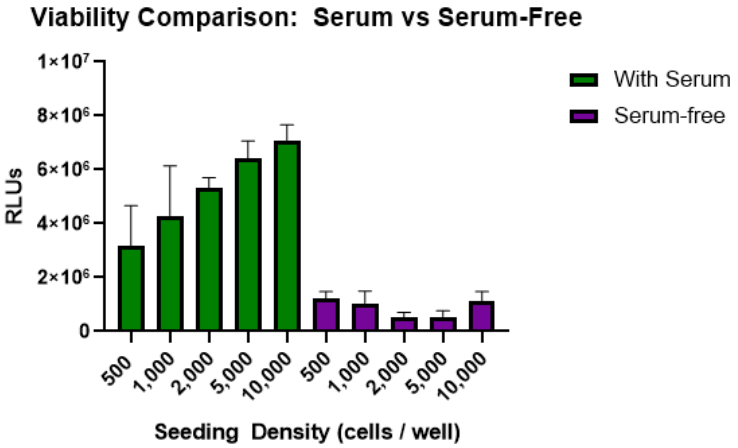

Figure 2. Comparing spheroid viability in different media conditions. Spheroids of different seeding densities were either maintained in FBS or transitioned to serum-free media. RLUs refers to relative luminescent units, i.e. the intensity of luminescence induced as a result of cellular ATP facilitating reaction with luciferase, thus reflecting cellular viability. 12 replicates were evaluated for each sample; error bars are representative of 95% confidence interval.

When comparing spheroids maintained in serum to spheroids transitioned from serum to serum-free conditions over a period of 5 days, we noted that spheroid viability decreased

when transitioned to serum-free conditions, regardless of seeding density (**Figure 2**). Additionally, spheroids of larger seeding densities appeared to have more irregular, asymmetric morphology than spheroids of smaller seeding densities (**Figure 3**). In order to culture spheroids with simple spherical morphology, and to decrease overall area of a necrotic core, we selected 1,000 – 5,000 cell seeding density range for future work.

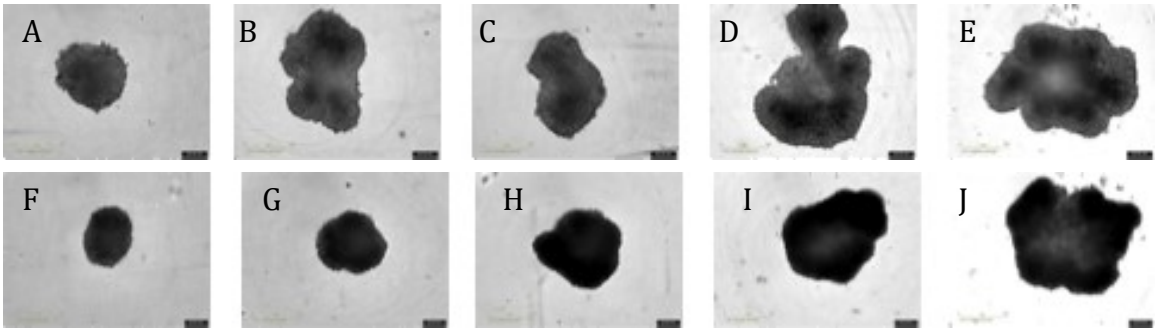

Figure 3. A visual comparison of spheroid morphology collected via Incucyte imaging. Panels A-E are HepG2 spheroids of different seeding densities (500, 1,000, 2,000, 5,000, and 10,000 cells/well) maintained in media with constant levels of fetal bovine serum. Panels F-J are HepG2 spheroids of different seeding densities (500, 1,000, 2,000, 5,000, and 10,000 cells/well) maintained in serum-free media. Lower right hand bar is time-stamp. Spheroids were cultured in 12 replicates.

A comparison of HepG2 spheroids cultured in media containing FBS or media containing HS, revealed different apparent spheroid densities - as exhibited by color differences in **Figure 4.** Some previous research has suggested that coloration is a reflection of spheroid density, *i.e.* darker appearance corresponds with more cells [23], however, this was not reflected in cellular viability evaluation (**Figure 5**).

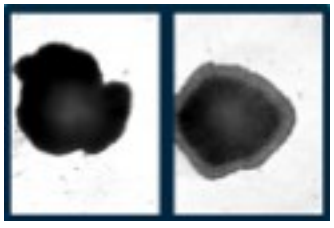

Figure 4. Different apparent spheroid densities. Images collected via Incucyte imaging.
Left: HepG2 spheroid cultured in FBS.
Right: HepG2 spheroid cultured in HS

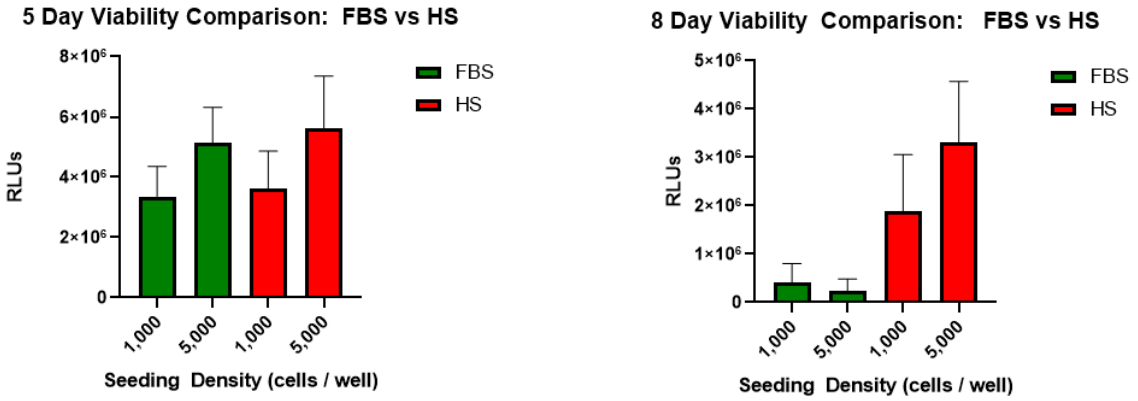

Figure 5. Monitoring spheroid viability after culture in Fetal Bovine Serum (FBS) and Human Serum (HS) conditions. After 5 days in culture spheroids have comparable viability regardless of culture conditions. After 8 days in culture there appear to be significant differences in spheroid viability, however both have declined markedly. RLUs refers to relative luminescent units, i.e. the intensity of luminescence induced as a result of cellular ATP facilitating reaction with luciferase, thus reflecting cellular viability. 10 replicates were evaluated for each sample; error bars are representative of 95% confidence interval

Regardless, HepG2 spheroid morphology remained consistently "compact aggregate" independent of changes in culture conditions. Over a five-day period, HepG2 spheroids cultured in either FBS or HS exhibited comparable viability values, as shown in **Figure 5**. Viability was also consistent with different spheroid seeding densities – HepG2 spheroids seeded at 1,000 cells per well had less overall luminescence signal than spheroids seeded at 5,000 cells per well, indicating a higher number of overall cells in the larger seeding density. This suggests that the necrotic core is not impacting the overall viability of the spheroids, i.e. both 1,000 and 5,000 cell seeding densities do not illustrate significant interference due to necrosis. When evaluated after 8 days in culture, spheroids cultured in both FBS and HS demonstrated a decrease in viability; however, spheroids cultured in FBS appear to decrease more than spheroids cultured in HS (**Figure 5**). These results suggest that if HepG2 spheroids are going to be used for any

experimentation for eight days or more, it is beneficial to consider culture in media containing HS.

To examine if HS conditions impacted transfection of spheroids with LNPs, as suggested through the lipid metabolism findings by Pramfalk *et al*., spheroids were transfected with LNPs containing enhanced Green Fluorescent Protein (eGFP) mRNA, and resulting eGFP expression was measured using an IncuCyte high-content fluorescent microscope housed in a cell culturing incubator. Using the IncuCyte to measure fluorescence allowed quantitation of eGFP expression in near real time, while cells were kept in their optimal environment. Transfection with eGFP LNPs was monitored immediately following dosage, with expression detected as early as 8 hours post-transfection (**Figure 6**). Maximum eGFP expression was attained at approximately 48 hours, with additional time expression increased only marginally and in a dose-dependent fashion

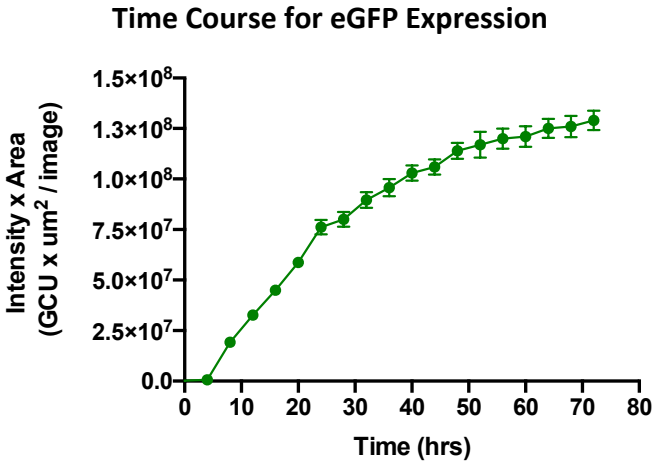

Figure 6. Time course for eGFP expression in HepG2 3D spheroids following administration of a 500 ng mRNA dose. Protein expression was measured in near real time via Incucyte imaging. 15 replicates were evaluated for each sample; error bars are representative of 95% confidence interval

Examination of eGFP LNP dose response in media containing FBS shows significant toxicity in the high dose of 2000 ng mRNA, resulting in a large hook (**Figure 7**). Minor toxicity accompanied the 1000 ng mRNA dose, with the 500 ng mRNA dose exhibiting the highest expression without toxicity. These results suggest that optimal mRNA dosage must be identified to target the desired range of protein expression following LNP administration.

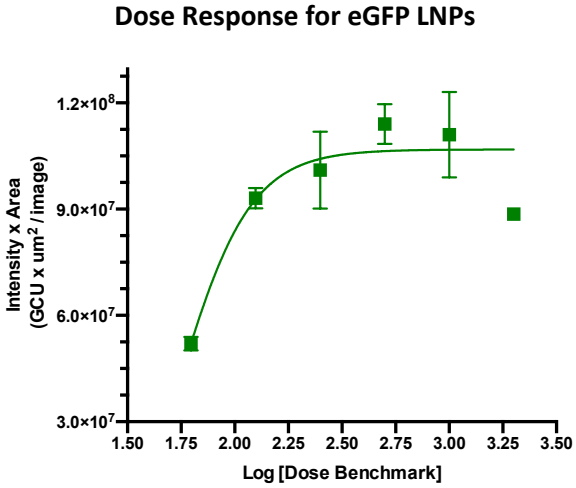

Figure 7. Dose response for eGFP LNPs in HepG2 3D spheroids cultured in media containing FBS. Hook effect is evident. Data shown is from 1 replicate evaluated; error bars are representative of 95% confidence interval

After maximum eGFP expression was observed, cells were measured for post-transfection viability. Post-transfection viability was comparable across seeding densities and between FBS and HS conditions (**Figure 8**). This suggests that overall spheroid viability post-transfection was not adversely impacted by either media condition.

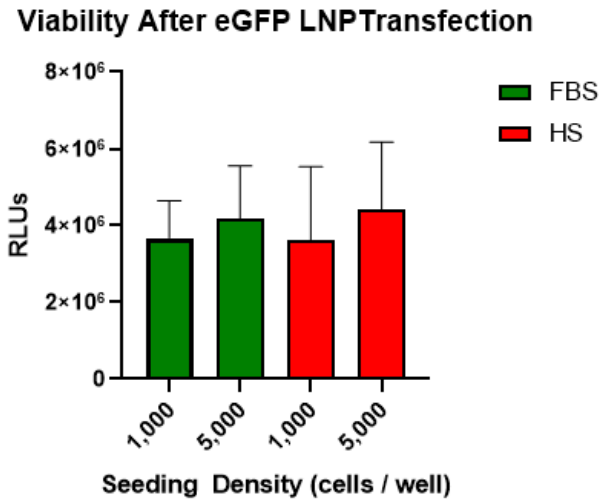

Figure 8. Comparing spheroid viability after transfection with eGFP LNPs. RLUs refers to relative luminescent units, i.e. the intensity of luminescence induced as a result of cellular ATP facilitating reaction with luciferase, thus reflecting cellular viability. 15 replicates were evaluated for each sample; error bars are representative of 95% confidence interval

However, upon closer examination of different eGFP LNP dosages to HepG2 spheroids in different culture conditions, some LNP transfection-induced cytotoxicity is evident (**Figure 9**). For spheroids cultured in media containing FBS, cytotoxicity was observed with the highest 2000 ng mRNA dose, but at lower concentrations eGFP was expressed in a dose dependent fashion. For spheroids cultured in media containing HS, there was no evident cytotoxicity. At the 2000 ng, the highest levels of eGFP expression were observed, however lower dosages showed much lower eGFP expression than seen in the FBS counterpart. These results suggest that in HS media conditions, eGFP LNPs are much less potent (*i.e.* a larger dose is required for a comparable response).

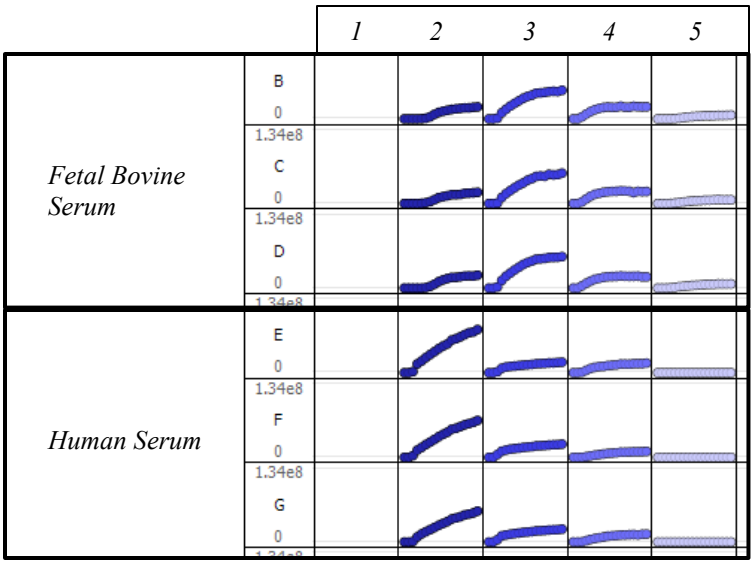

Figure 9. Green fluorescence intensity over 48 hour time interval as shown via plate layout. Column 1 was an untransfected control, column 2-5 were transfected with 2000,1000, 500, and 250 ng mRNA doses respectively. Experiments were later performed for additional trials with similar results.

Via compilation of dose response curves, potency values for LNPs in different media conditions were calculated. **Figure 10** shows that transfection in media containing HS is significantly less potent than transfection in media with FBS. This data, with the findings from Figure 9, illustrate that transfection in HS is less potent and less dose dependent than transfection in FBS media.

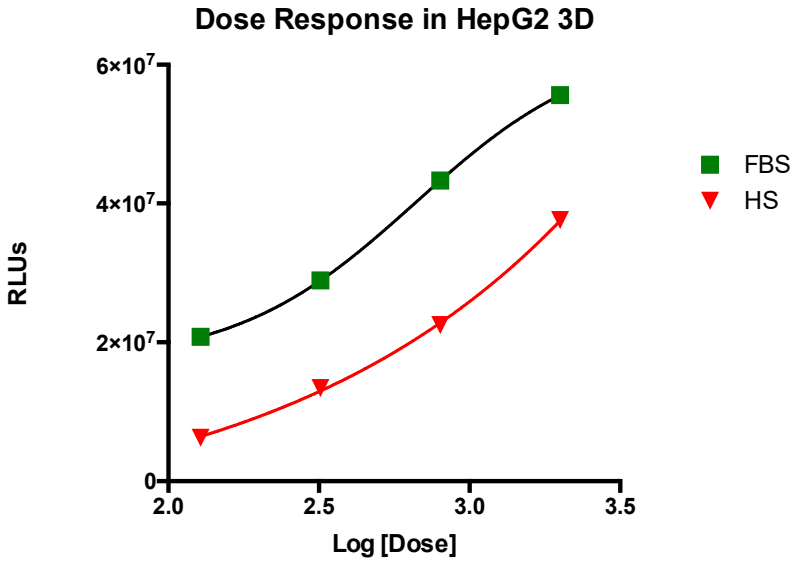

Figure 10. Dose response for HepG2 3D spheroids in media containing FBS or HS. A rough calculated EC_{50} for the FBS condition is 662 ng mRNA, and 8e10 for the HS condition, highlighting markedly lower potency associated with HS.

Timed imaging showed eGFP activity penetrating inward from the perimeter of the spheroid (Video in **Supplemental Figures**), which is logical, as the spheroid perimeter is directly exposed to the solution containing LNPs. HepG2 spheroid morphology after transfection with eGFP LNPs is shown in **Figure 11**. Spheroids did not dissociate with any LNP dosage, remaining distinctly compact aggregate. Figure 11 also demonstrates higher fluorescent intensity in the perimeter of the spheroid, as compared to the core, again illustrating transfection starting at the spheroid perimeter and eventually bleeding towards the center.

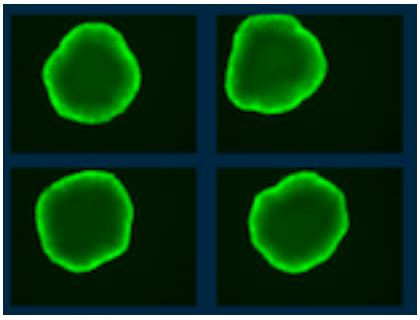

Figure 11. HepG2 spheroids (maintained in media with FBS, 5,000 cells / well) 48 hours after eGFP LNP transfection. "Compact aggregate" morphology is evident. Cells are from plate shown in Figure 9, treated with 1000 ng and 500 ng respectively. Images collected via Incucyte imaging. Spheroids approximated 1000 μm in diameter.

Since culture and maintenance of spheroids in HS did not exhibit more "spheroidal" morphology or increased viability than spheroids cultured and maintained in FBS, and an FBS/HS comparison showed lower potency and less dose-dependence in media containing HS, we proceeded with FBS for culture. Additionally, as the transition to serum-free conditions adversely impacted spheroid viability without significant improvement in spheroid morphology, we decided to conduct spheroid culture in medium with constant levels of FBS (i.e. no transition to serum-free). FBS is commonly used in cell culture technique, widely available, and relatively inexpensive, thus this decision supports an accessible and high-throughput methodology for future use.

b. Immortalized Hepatocellular Cell Line: Hep3bs

Although HepG2s and Hep3bs are both derived from hepatocytes, they show significantly different protein expression (identity and levels) from human liver models and each other [26,27]. This suggests that experimentation with HepG2 and Hep3b cells may yield different results when examining a potential *IVIVC*. Furthermore, HepG2 and Hep3bs cells are often used in mechanistic studies to understand drug metabolism [28].

In order to adapt our 3D spheroid protocol for HepG2s to Hep3bs, we cultured Hep3bs in similar conditions to HepG2s. The only adaptations to our protocol were changes to base media composition specific for Hep3bs, but FBS was maintained at the same concentration as HepG2 culture. Cultured Hep3bs formed spheroids within 24-48 hours, exhibiting tighter, more compact structure than HepG2 spheroids (**Figure 11** and **Figure 12**). Moreover, eGFP expression timing and patterns in Hep3b spheroids were similar to HepG2s, with detectable levels of expression observed starting at 8 hours and plateauing by 48 hours.

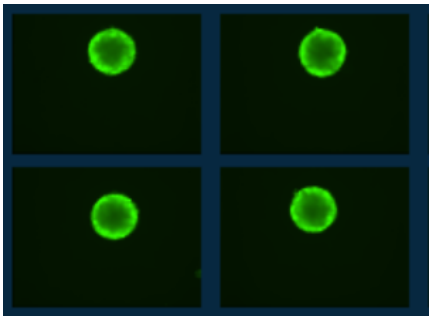

Figure 12. Hep3b spheroids (maintained in media with FBS, 3,000 cells / well) 48 hours after eGFP LNP transfection. Morphology is distinctly spheroidal. Images collected via Incucyte imaging. Spheroids approximated 600 μm in diameter.

c. Primary Human Hepatocytes

Primary human hepatocyte spheroids were cultured directly from cryopreservation according to the manufacturer's protocol, as described in the Methods section

above. These spheroids exhibited "compact aggregate" morphology with an observable number of satellite cells that did not participate in spheroid formation **(Figure 13)**. We believe that these satellite cells are not viable cells, as total viability of primary human hepatocytes following thaw from cryopreservation is typically between 70 and 80%. Efforts were made to monitor satellite cell viability via Annexin Red, however PHH autofluorescence was noted as a confounding factor (shown in **Supplemental Figures)**. PHH also exhibited autofluorescence under green light, and were therefore not transfected with eGFP LNPs to visualize LNP transfection through the spheroid. For additional studies with PHH, we used luciferase mRNA instead of eGFP to eliminate any interference from autofluorescnce.

.

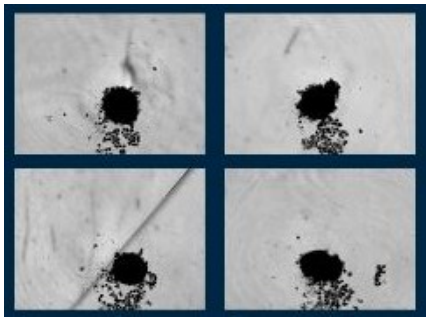

Figure 13. Primary Human Hepatocyte spheroids (2,000 cells / well) . Morphology shows distinct compact aggregate with some separate satellite cell colonies. Images collected via Incucyte imaging. Spheroids approximated 500 µm in diameter.

II. Lipid Nanoparticle Design

a. Standard LNPs

In order to thoroughly test different LNP compositions within our 2D, 3D, and in vivo models, we designed a set of standard LNPs that consist of PEG-DMG, cholesterol, helper lipid, and ionizable lipid in ratios that have previously shown to be effective. By varying the helper lipid, we sought to examine differences in LNP transfection efficiencies previously described by Kulkarni *et al* [10]. Kulkarni *et al.* showed that an unsaturated helper lipid (DOPC) performed better than a saturated helper lipid (DSPC) *in*

vitro, but the opposite was true with transfections *in vivo* [10]. By maintaining PEG-DMG, cholesterol, and ionizable lipid identity and ratios constant and varying the identity of helper lipids, we aimed to clarify these contradictory results. We sought to confirm that DOPC and DSPC performed differently when evaluated in traditional 2D culture versus *in vivo* models, and to examine if 3D culture could bridge this gap. Within our set of standard LNPs, LNP A1 serves as our positive control, as it is known as the "benchmark" formulation within the field [2,4,10].

Table 1. Composition of Standard LNP Formulations

	Ionizable Lipid (%)	**Helper Lipid (%)**	**Cholesterol (%)**	**DMG-PEG (%)**
A1	DLinMC3DMA (50.0%)	DSPC (10.0%)	38.5%	1.5%
A2	DLinMC3DMA (50.0%)	DOPC (10.0%)	38.5%	1.5%
A3	DLinMC3DMA (50.0%)	DOPE (10.0%)	38.5%	1.5%
A4	DLinMC3DMA (50.0%)	SOPC (10.0%)	38.5%	1.5%
A5	DLinMC3DMA (50.0%)	Cholesterol (10.0%)	38.5%	1.5%

b. Non-Standard LNPs

Our non-standard LNPs maintain cholesterol, DMG-PEG, and helper lipid ratios and identities, while varying a combination of ionizable lipids. The ionizable lipid combination includes varying amounts of DLinMC3DMA (MC3) and 1,2-dioleoyl-3-(trimethylammonium) propane (DOTAP). MC3 is the newest "gold standard" for ionizable lipids, however, previously DOTAP was widely used due to its complexing cationic head group and biodegradable character [29,30]. Via combination of MC3 and DOTAP, we hope to amplify the favorable qualities of both molecules (complexation,

biodegradation), while minimizing the drawbacks associated with individual molecules (toxicity).

Other combinatory lipid nanoparticles have been examined, particularly combining lipid and polymer groups. With some hybrid lipid-polymer nanoparticles, increased transfection efficiency is observed [29,31]. We hypothesize that a combinatory lipid-lipid nanoparticle, may exhibit increased transfection efficiency.

Table 2. Composition of Non-Standard LNPs

	Ionizable Lipid (%)	**Helper Lipid (%)**	**Cholesterol (%)**	**DMG-PEG (%)**
MX1	DLinMC3DMA (25.0%) DOTAP (25.-%)	DSPC (10.0%)	38.5%	1.5%
MX2	DLinMC3DMA (40.0%) DOTAP (10.0%)	DSPC (10.0%)	38.5%	1.5%
MX3	DLinMC3DMA (10.0%) DOTAP (40.0%)	DSPC (10.0%)	38.5%	1.5%
MX4	DOTAP (50.0%)	DSPC (10.0%)	38.5%	1.5%

III. Head to Head Comparison of LNPs In Vitro

Standard and non-standard LNP formulations loaded with luciferase mRNA were tested in 2D and 3D cell cultures across HepG2s, Hep3bs, and PHH, in order to evaluate a possible correlation between behavior in 3D and later LNP performance in vivo. Luciferase expression was measured by luminescence 24 hours after each transfection, and results were plotted against mRNA concentration in order to calculate EC_{50} and E_{max} values to describe potency and

maximum expression, respectively. With comparison of EC_{50} values across LNP formulations and cell culture methods, LNP A1 exhibited a consistently higher potency (lower EC_{50}) than other LNPs across all cell lines and conditions, except for PHH 2D and 3D (**Table 3, Figure 14)**. These results are consistent with LNP A1's composition and its status as a "benchmark" formulation for previous *in vitro*, 2D culture studies.

Table 3. EC_{50} values (ng mRNA) for standard LNPs across cell and culture type.

	A1	A2	A3	A4	A5
HepG2 2D	44.64	237.4	216.1	127.3	197.1
HepG2 3D	50.38	206.8	112.3	243.6	135.4
Hep3b 2D	67.53	199.7	127.1	274.7	140.6
Hep3b 3D	81.15	371.5	304.7	165.6	449.3
PHH 2D	60.22	33.12	41.69	56.98	3.3**
PHH 3D	182.7	188.4	188.4	137.6	219.7

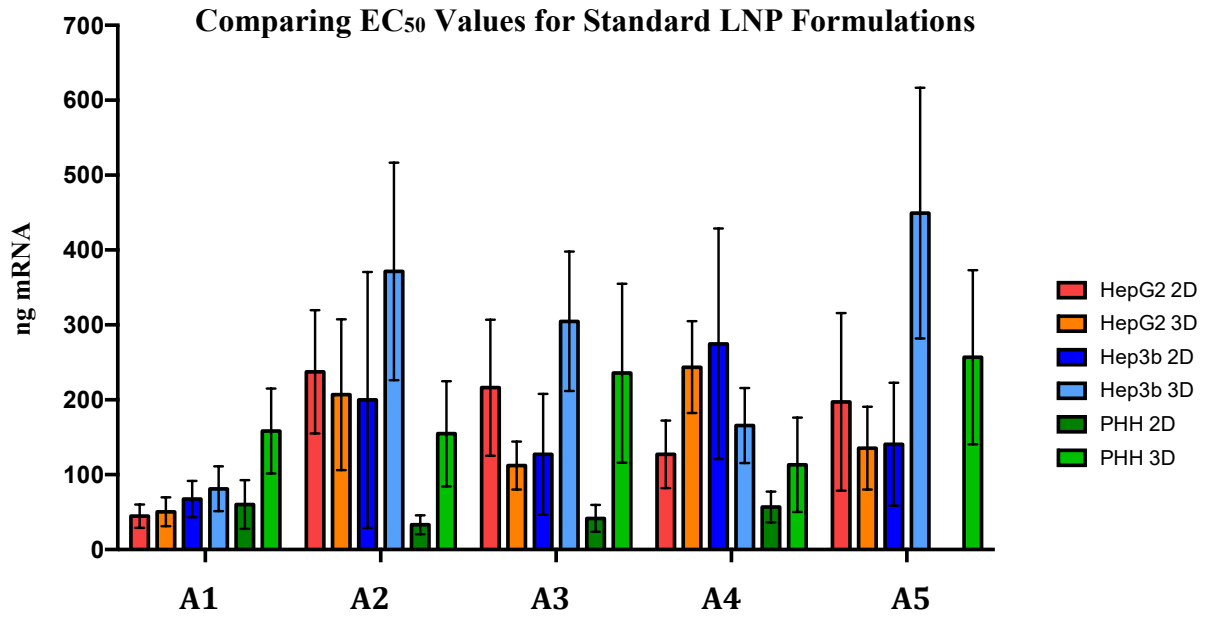

Figure 14. A comparison of EC_{50} values by cell and culture type across each standard LNP formulation. LNP A1 is known as the "benchmark" within the field, and accordingly exhibits consistently low EC_{50} values. The calculated value for LNP A5 in PHH 2D was noted to be extremely low and likely inaccurate. In 2D culture 7 replicates were tested, in 3D culture 10 replicates were tested. Data is from 3 separate trials. Error bars represent 95% confidence interval.

For standard LNP formulations, an increase in EC_{50} values is observed in PHH from 2D to 3D culture conditions. In four of five standard LNP formulations, EC_{50} values also increase from 2D to 3D culture in Hep3bs. This is consistent with a higher dose necessary for a desired effect when transitioning from cellular monolayers or more complex structures. Since PHH in 2D culture are considered the gold standard for their likeness to originating tissues [13,14], these results are promising. With HepG2s, however, there is no apparent trend with the transition from 2D to 3D culture. This lack of transition may be due to HepG2s forming loose aggregates in 3D cultures, as opposed to tighter spheroid formations observed with Hep3b and PHH 3D cultures.

Evaluation of non-standard LNP formulations does not reveal any trends with EC_{50} values in relation to culture or cell type (**Table 4** and **Figure 15**). This suggests that transfection results are highly dependent on both cell type and LNP formulation.

Table 4. EC50 values (ng mRNA) for non-standard LNPs across cell and culture type. For some formulations, it was not possible to determine EC50 values due to low efficacy.

	MX1	**MX2**	**MX3**	**MX4**
HepG2 2D	120.8	655.1	443.8	------
HepG2 3D	110.5	1329	------	724.1
Hep3b 2D	275.2	678.3	2221	------
Hep3b 3D	552.1	1396	3494	------
PHH 2D	1362	702.9	707.3	1066
PHH 3D	1471	3003	------	------

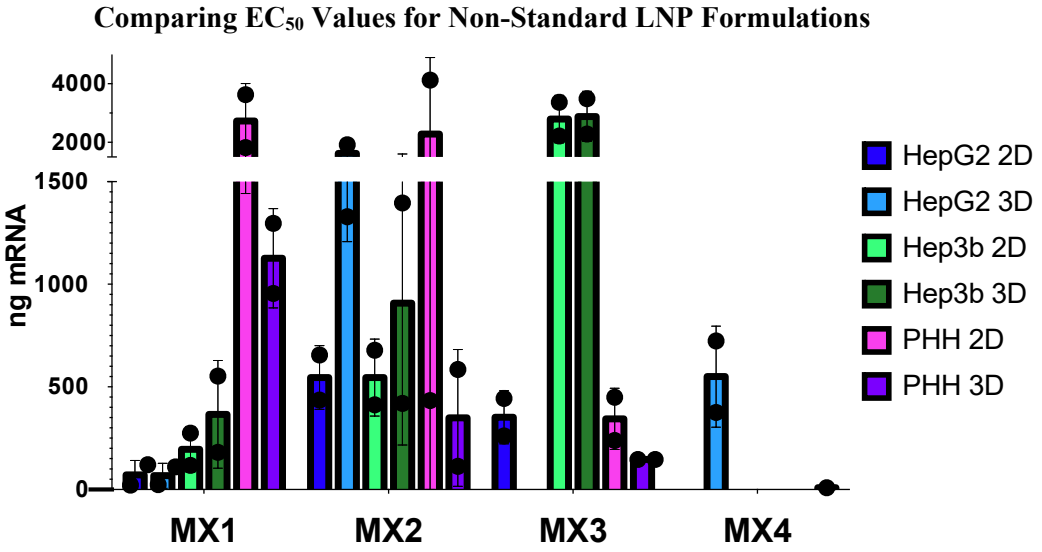

Figure 15. A comparison of EC_{50} values by cell and culture type across each non-standard LNP formulation. Data points for several transfections were not able to be determined due to low LNP efficacy. In 2D culture 7 replicates were tested, in 3D culture 10 replicates were tested. Data is from 3 separate trials. Error bars represent 95% confidence interval.

To further analyze LNP performance, E_{max} values were calculated. Comparing maximum expression values of LNPs at a singular dose is often used to identify well-performing LNPs [10,22,32], and thus is a metric that should also be considered in our IVIVC search [10,32]. Luminescence counts associated with expression of luciferase mRNA were normalized to LNP A1 as the "benchmark" formulation, so to normalize cell number and growth differences between HepG2, Hep3b, and PHH that influence absolute luciferase expression. In the context of Kulkarni et al.'s results, LNP A1 contains unsaturated helper lipid DOPC, whereas LNP A2 contains saturated helper lipid DSPC. For our transfections in HepG2 cells (2D and 3D), LNP A2 exhibits a higher maximum expression than LNP A1 (**Figure 16**). When evaluating only E_{max} values, these results show that LNP A2 has higher mRNA expression than LNP A1, and could thus be assumed to be more effective, both in 2D and 3D culture. However, A2

demonstrated lower potency than A1, as previously mentioned, which also plays a significant role in in vivo transfection efficiency.

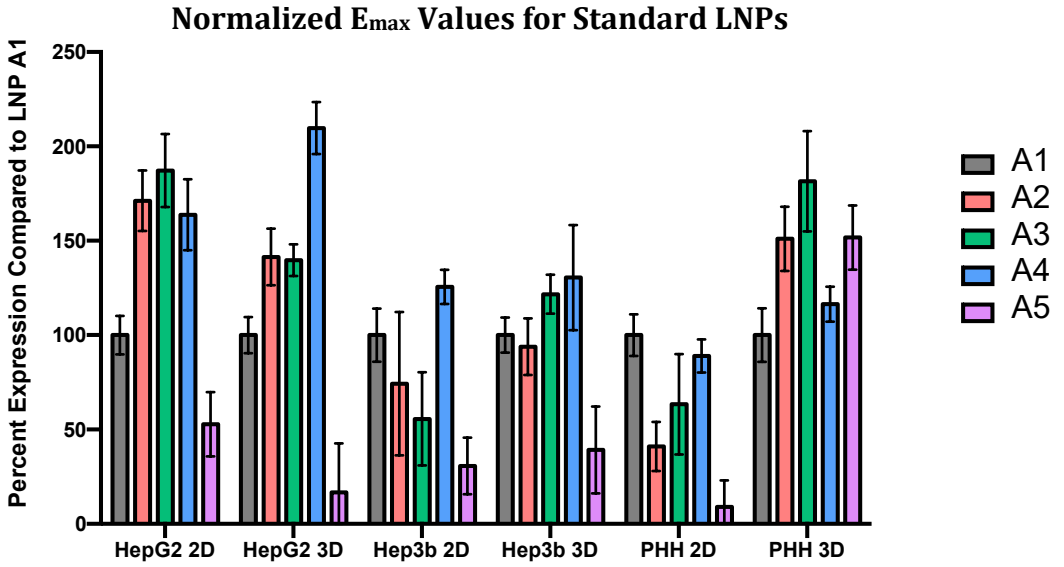

Figure 16. Normalized E_{max} values for standard LNPs as compared to LNP A1. Each cell and culture type tested is shown. In 2D culture 7 replicates were tested, in 3D culture 10 replicates were tested. Data is from 3 separate trials. Error bars represent 95% confidence interval.

Examining 2D and 3D culture E_{max} results across cell types does not highlight any readily evident trends – E_{max} values were sometimes decreased with the transition from 2D to 3D culture, and other times increased or remained relatively constant. PHH 2D cells, the gold-standard for toxicity studies [14], showed higher expression in LNP A1 than any other standard formulation. However, PHH 3D cells showed higher expression with LNPs A2-A5 than with LNP A1. This suggests that PHH in 3D culture are significantly different than PHH in 2D culture, however, the question remains which is more indicative of *in vivo* results.

When considering normalized E_{max} values for non-standard LNPs, there are also few obvious trends (**Figure 17**). LNP MX1 and MX2 successfully transfected each culture type, but seem to show highly variability in eMax values across cell and culture types. Interestingly, LNP MX4 only appears to significantly transect PHH in 2D culture. Altogether, the non-standard LNPs seem to have high expression values in PHH.

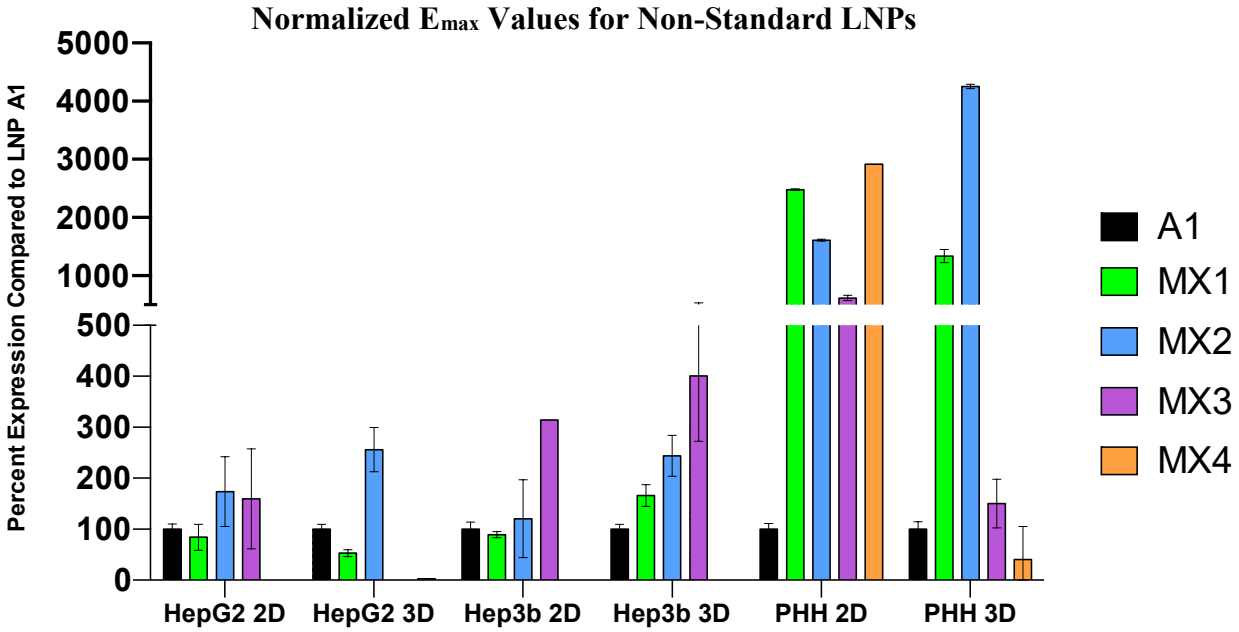

Figure 17. Normalized E_{max} values for non-standard LNPs as compared to LNP A1. Each cell and culture type tested is shown. For unsuccessful transfections, no data is shown. In 2D culture 7 replicates were tested, in 3D culture 10 replicates were tested. Data is from 3 separate trials. Error bars represent 95% confidence interval.

By considering E_{max} values alone, LNP MX1 seems as if it might be promising for further experimentation. However, when EC_{50} values for LNP MX1 are also considered (**Table 4**), it is evident that this LNP has very low potency. This suggests that it may be valuable to evaluate LNPs on more than one metric – as high expression does not always correspond with high potency, and vice versa.

IV. Head to Head Comparisons of LNPs In Vivo

Significant differences in LNP potency and maximum expression were observed with variation of cell and culture types. LNP transfections within PHH 2D as compared to PHH 3D even demonstrated clear differences in regards to potency and efficacy. Thus, the *in vivo* translatability of cell type and 2D versus 3D culturing remains unclear without conducting an *in vivo* study. As part of an ongoing study, we selected our standard LNP formulations and a negative control to administer to balbC mice. Our LNPs were loaded with a specific mRNA that encodes for therapeutic antibody expression that is easily quantified in mouse serum.

The selected LNPs were formulated as described in Methods, then administered to HepG2, Hep3b, and PHH cells in 2D and 3D culture, along with the balbC mice. Transfection and viability data were collected for all cell and culture types, and *in vivo* data is pending.

Conclusions and Future Work

By establishing a rigorous protocol for the culture of HepG2 and Hep3b 3D spheroids, with emphasis on seeding density and culture media conditions, we examined a possible IVIVC. Manipulating the composition of LNPs showed how some variations in LNP structure impact transfection in certain conditions. With our standard LNP formulations, helper lipid identity impacts LNP transfection in all cell and culture types. For example, transfection with LNP A5 resulted in less potent transfection as compared to the benchmark LNP A1 as a direct result of direct substitution of the helper lipid. From our research thus far, it is apparent that LNPs perform differently in different cell types and culture conditions. Potency and maximum expression were not always congruous, emphasizing the need to evaluate LNPs on both metrics.

These results highlighted a wide array of *in vitro* results, and thus necessitate an *in vivo* study to clarify potential relationships. With our continued studies *in vivo* we hope to examine the relationship between transfection in 3D culture and *in vivo* models to determine if transfection in 3D culture is more predictive of *in vivo* transfection.

Supplemental Information

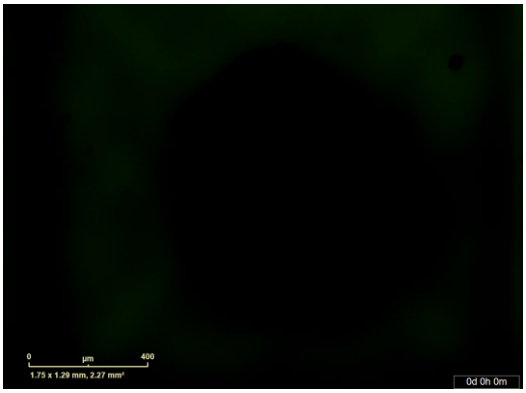

Supplemental Figure 1. Time-lapse video showing eGFP penetrating the perimeter of a HepG2 spheroid and moving inward. Images collected via Incucyte.

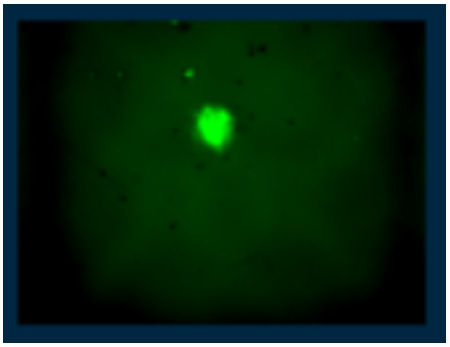

Supplemental Figure 2. Green autofluorescence of a PHH spheroid imaged via Incucyte.

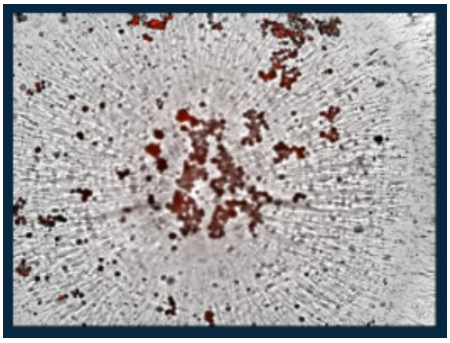

Supplemental Figure 3. Red autofluorescence of PHH cells seeded for spheroid formation as imaged via Incucyte.

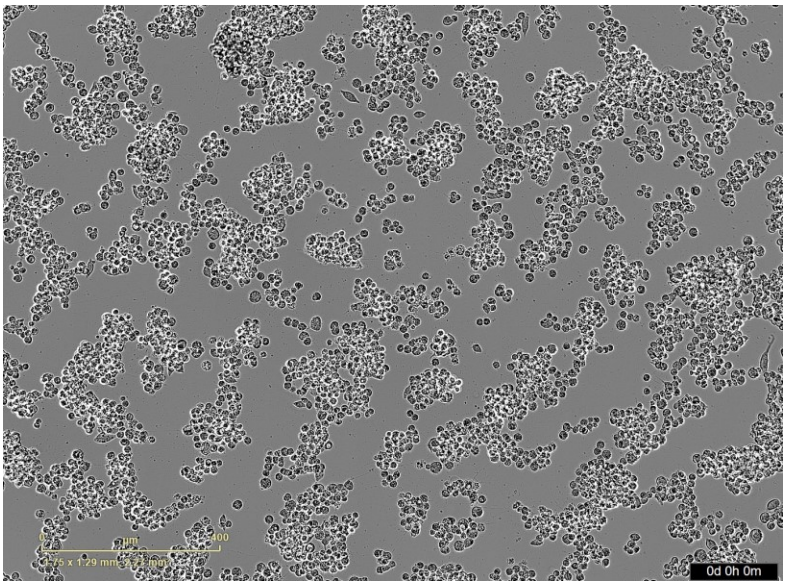

Supplementary Figure 4. HepG2 cells in 2D culture 24 hours post-transfection with LNPs containing 125 ng luciferase mRNA. Image collected via Incucyte.

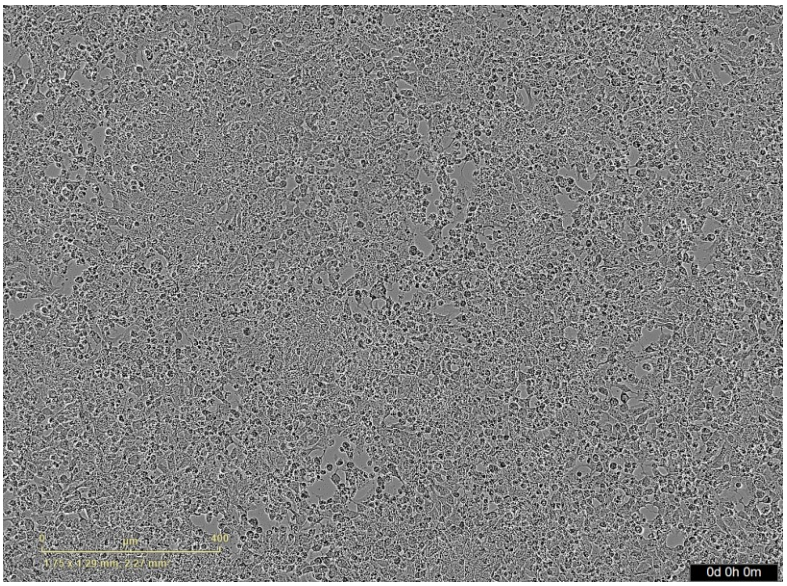

Supplementary Figure 5. Hep3b cells in 2D culture 24 hours post-transfection with LNPs containing 125 ng luciferase mRNA. Image collected via Incucyte.

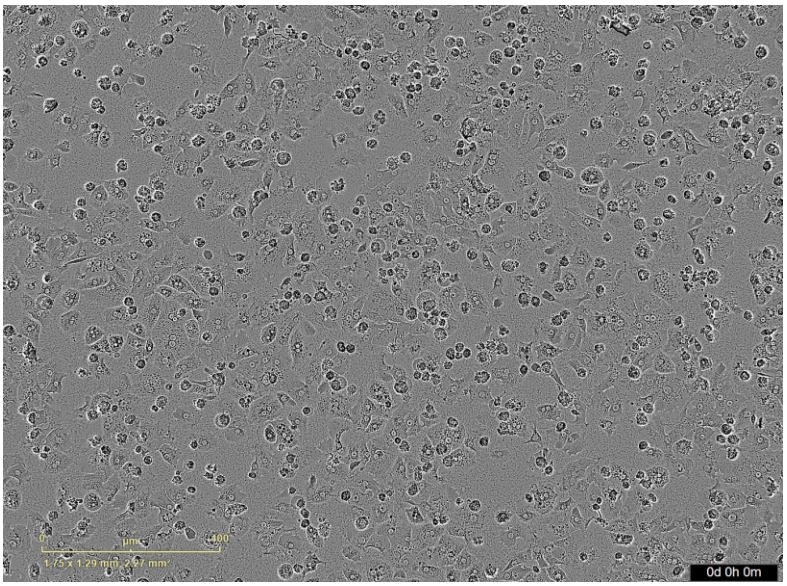

Supplementary Figure 6. Primary Human Hepatocytes in 2D culture 24 hours post-transfection with LNPs containing 125 ng luciferase mRNA. Image collected via Incucyte.

Supplemental Table 1. Dynamic Light Scattering data for LNP formulations.

	Average Size (nm)	Polydispersity Index	Zeta Potential (mV)
A1	63.14	0.03	-2.06
A2	68.14	0.05	-0.835
A3	72.49	0.05	-0.480
A4	63.52	0.04	-0.172
A5	70.27	0.02	-0.166
MX1	48.10	0.17	7.15
MX2	54.29	0.20	8.20
MX3	54.10	0.17	7.66
MX4	53.16	0.22	11.8

Supplemental Table 2. Average concentration and encapsulation efficiency of mRNA in LNP formulations as determined via Ribogreen Assay.

	Average mRNA in LNP (ug/mL)	Percent Encapsulation Efficiency
A1	310.8	84.7
A2	235.7	90.8
A3	287.6	92.1
A4	334.3	92.2
A5	324.2	96.7
MX1	305.2	98.4
MX2	261.1	75.4
MX3	185.6	98.9
MX4	232.1	98.5

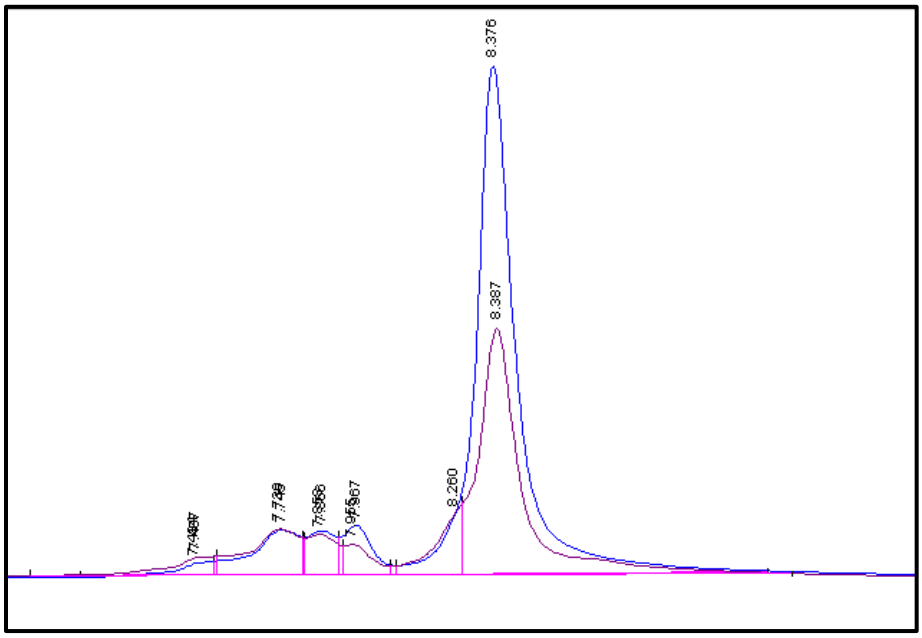

Supplemental Figure 7. RP-HPLC analysis for a luciferase mRNA control in comparison to encapsulated luciferase mRNA in LNP. This analysis was performed to monitor for potential mRNA degradation. Luciferase mRNA control is plotted in blue, LNP A5 is plotted in magenta. Aligned peaks suggest that

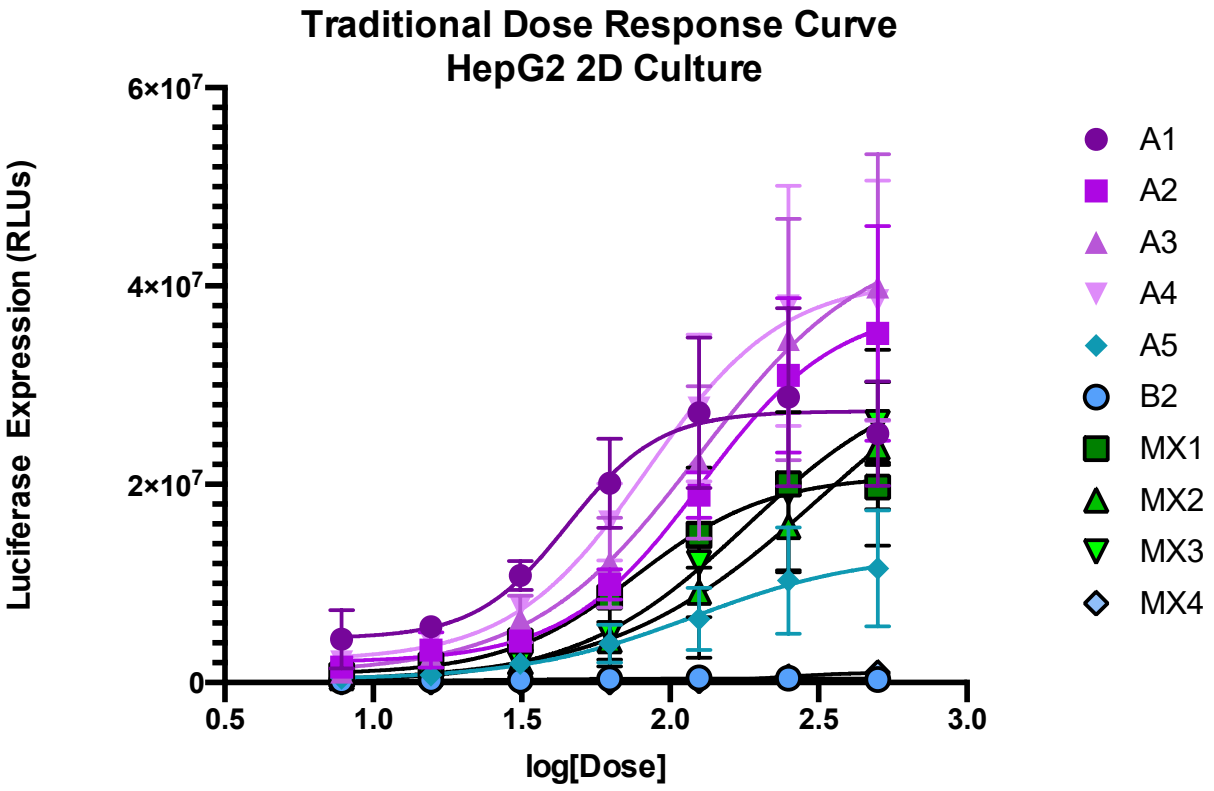

Supplemental Figure 8. Dose response curve for HepG2 2D culture. Difficult to attain meaningful and accurate EC50 values and resolution from this plot. Transitioned to Michaelis-Menten evaluation for further analysis.

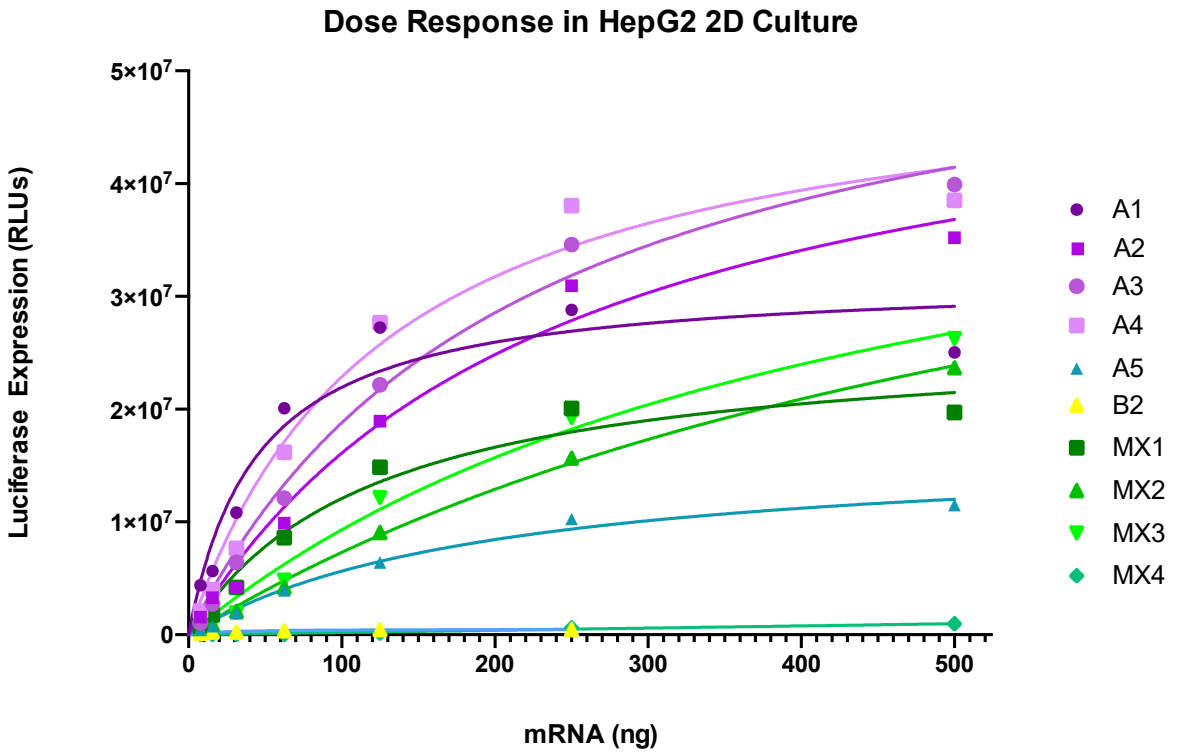

Supplemental Figure 9. Dose response data for LNP formulations in HepG2 2D culture. Any hook effects resulting from LNP toxicity were excluded. Plotted according to Michaelis-Menten, in order to attribute equal weigh to each data point. Kd values derived from this plot were used as EC50 values for data analysis.

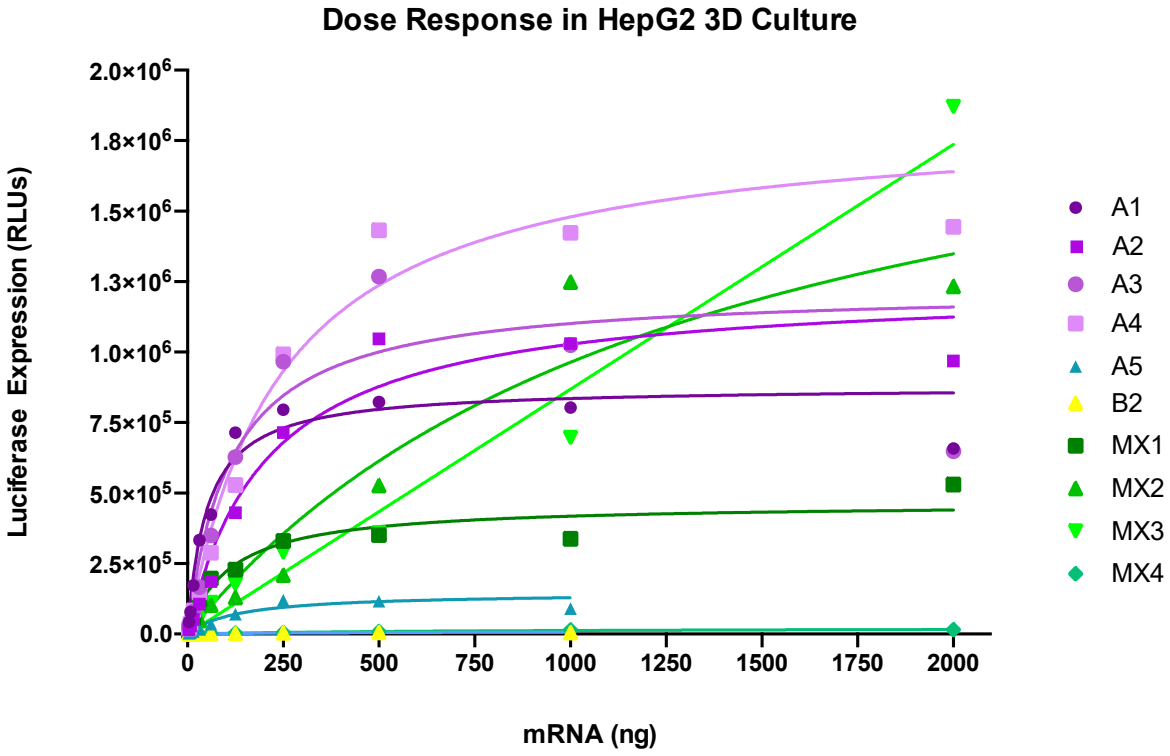

Supplemental Figure 10. Dose response data for LNP formulations in HepG2 3D culture. Any hook effects resulting from LNP toxicity were excluded. Plotted according to Michaelis-Menten, in order to attribute equal weigh to each data point. Kd values derived from this plot were used as EC50 values for data analysis.

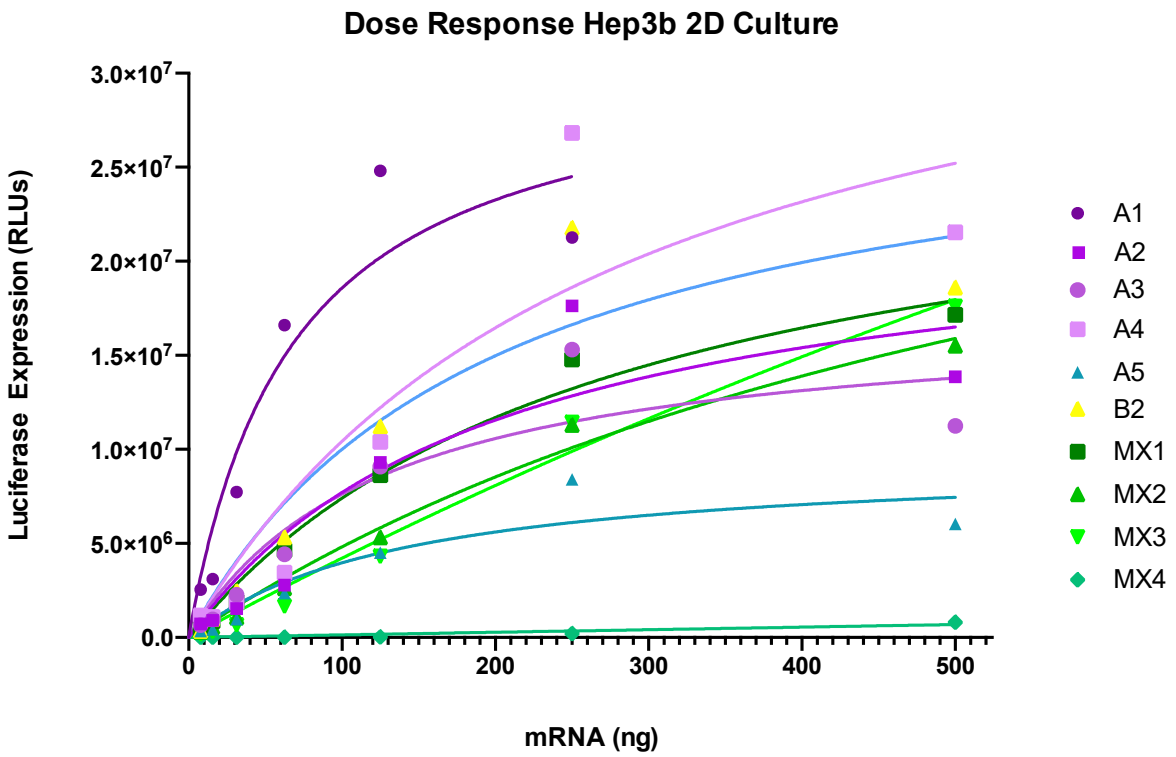

Supplemental Figure 11. Dose response data for LNP formulations in Hep3b 2D culture. Any hook effects resulting from LNP toxicity were excluded. Plotted according to Michaelis-Menten, in order to attribute equal weigh to each data point. Kd values derived from this plot were used as EC50 values for data analysis. Some activity from LNP B2 can be observed – LNP B2 serves as a negative control in all other cell types.

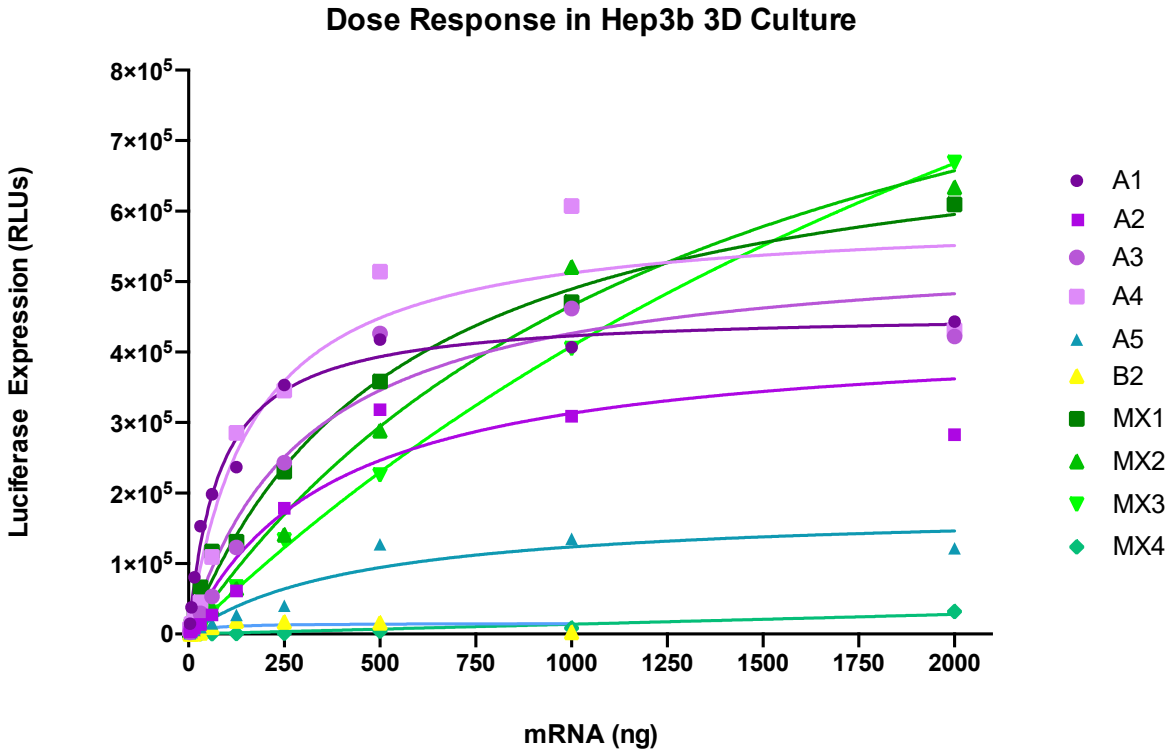

Supplemental Figure 12. Dose response data for LNP formulations in Hep3b 3D culture. Any hook effects resulting from LNP toxicity were excluded. Plotted according to Michaelis-Menten, in order to attribute equal weigh to each data point. Kd values derived from this plot were used as EC50 values for data analysis.

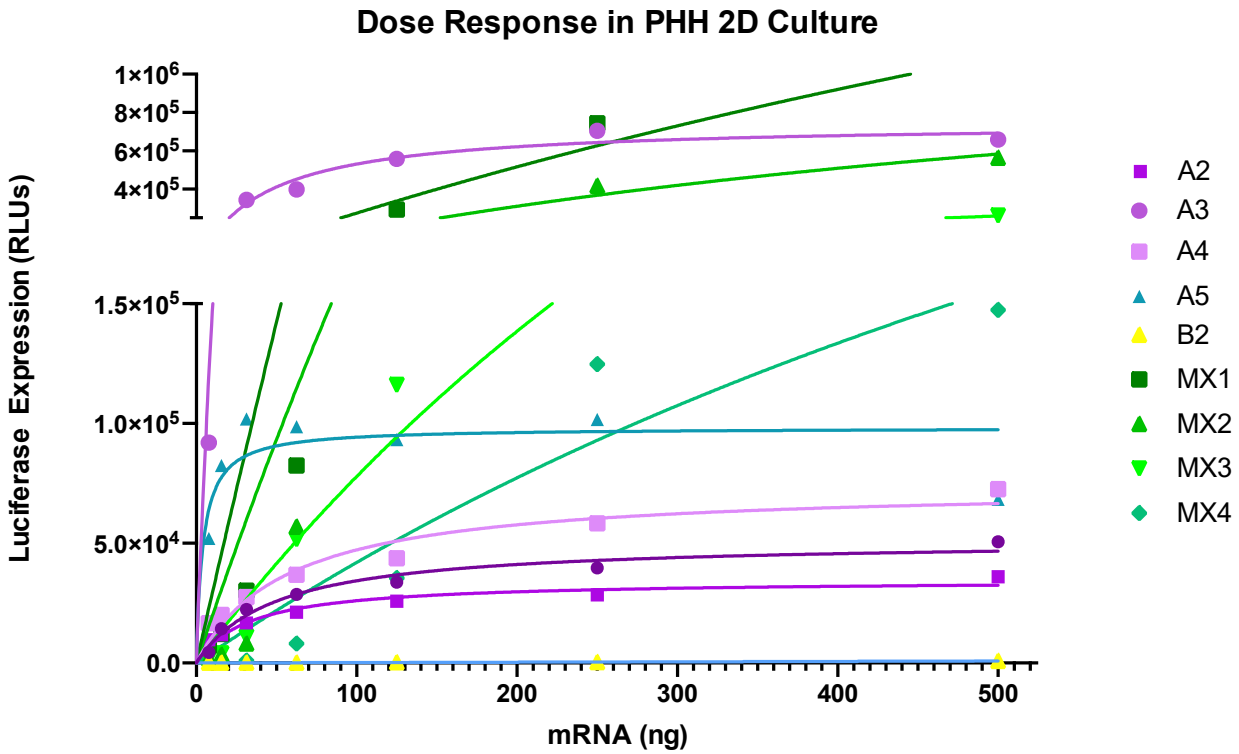

Supplemental Figure 13. Dose response data for LNP formulations in PHH 2D culture. Any hook effects resulting from LNP toxicity were excluded. Plotted according to Michaelis-Menten, in order to attribute equal weigh to each data point. Kd values derived from this plot were used as EC50 values for data analysis.

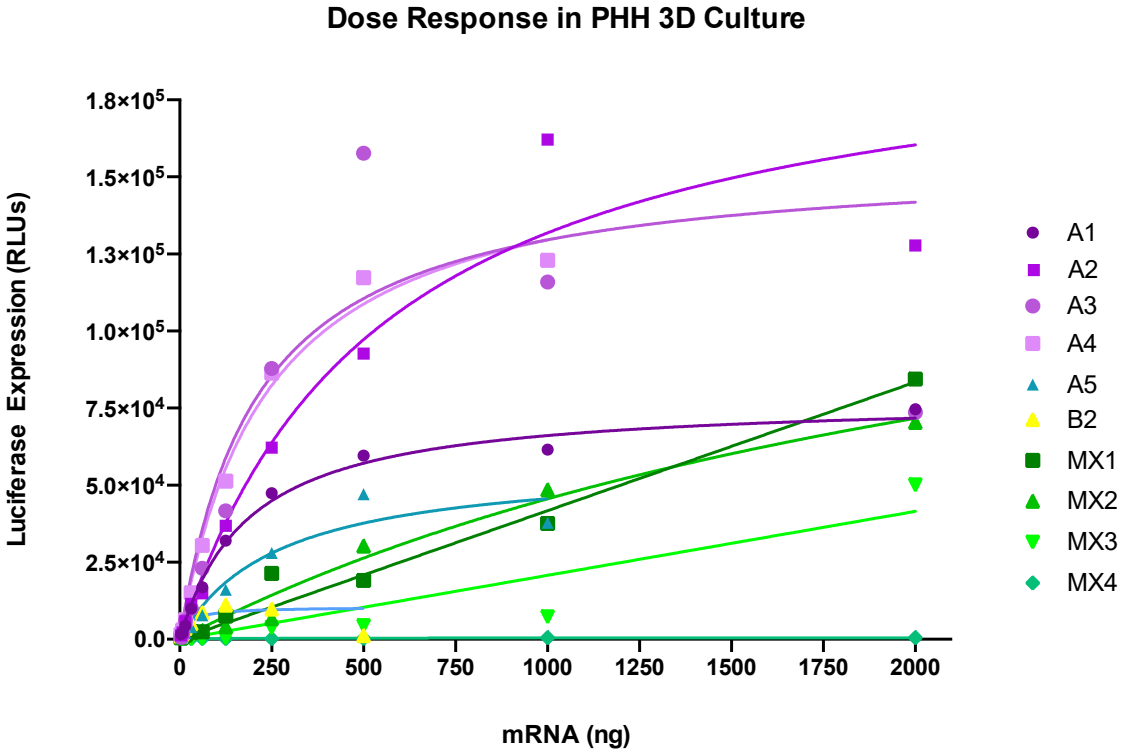

Supplemental Figure 14. Dose response data for LNP formulations in PHH 3D culture. Any hook effects resulting from LNP toxicity were excluded. Plotted according to Michaelis-Menten, in order to attribute equal weigh to each data point. Kd values derived from this plot were used as EC50 values for data analysis.

Comparing EC_{50} Values for Standard LNP Formulations

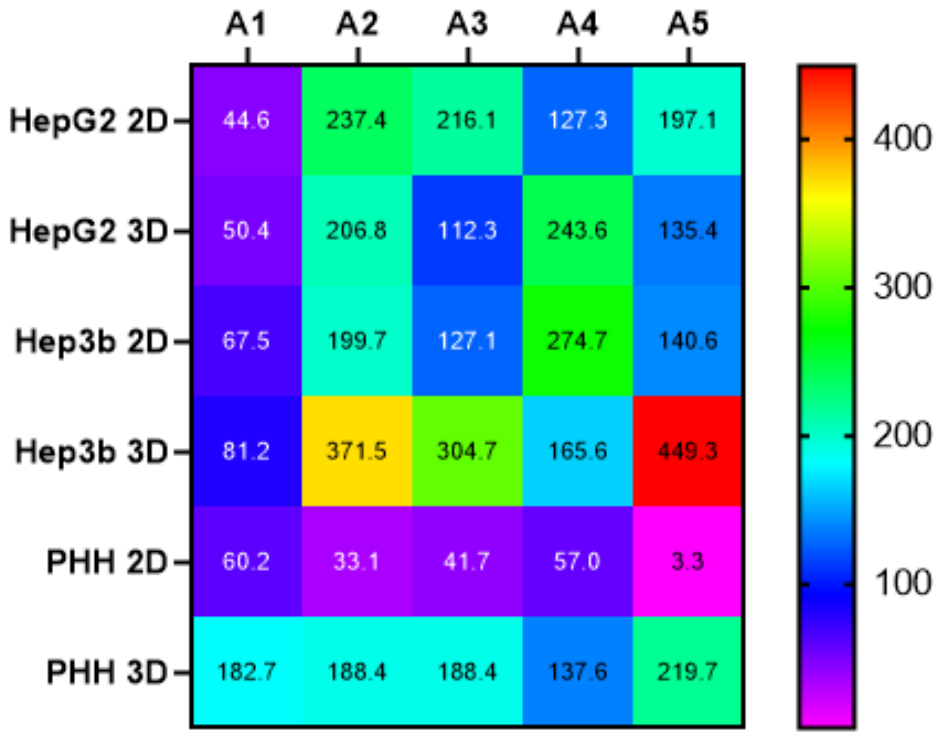

Supplemental Figure 15. Heat map of LNP standard formulation EC_{50} data. Note: LNP A5 in PHH 2D had an extremely low EC_{50} value – upon inspection of the dose response curve this data point was categorized as unreliable.

Comparing EC_{50} Values for Non-Standard LNP Formulations

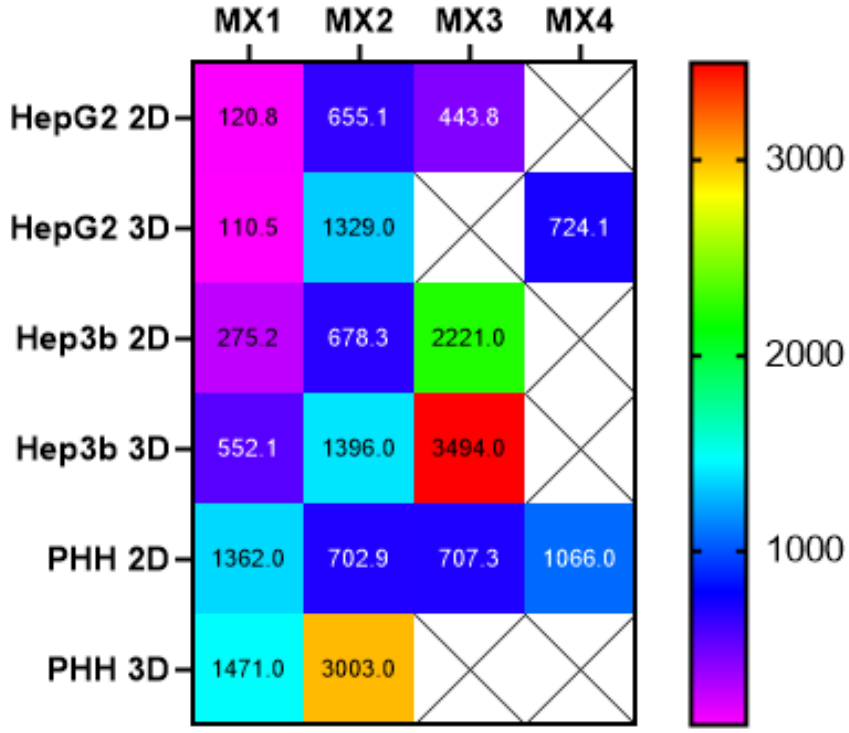

Supplemental Figure 16. Heat map of LNP non-standard formulation EC_{50} values. Boxes marked with an "x" denote transfections for which no EC_{50} could be determined.

References

1. Rui Y, Wilson DR, Green JJ. Non-Viral Delivery To Enable Genome Editing. *Trends Biotechnol*. 2019; 37: 281–293.

2. Cullis PR, Hope MJ. Lipid Nanoparticle Systems for Enabling Gene Therapies. *Mol Ther.* 2017; 25: 1467–1475.

3. Buck J, Grossen P, Cullis PR, Huwyler J, Witzigmann D. Lipid-Based DNA Therapeutics: Hallmarks of Non-Viral Gene Delivery. *ACS Nano*. 2019; 13: 3754–3782.

4. Yanez Arteta M, Kjellman T, Bartesaghi S, Wallin S, Wu X, Kvist AJ, et al. Successful reprogramming of cellular protein production through mRNA delivered by functionalized lipid nanoparticles. *Proc Natl Acad Sci*. 2018; 115: E3351–E3360.

5. Tam YYC, Chen S, Cullis PR. Advances in Lipid Nanoparticles for siRNA Delivery. *Pharmaceutics*. 2013; 5: 498–507.

6. Kauffman KJ, Robert Dorkin J, Yang JH, Heartlein MW, DeRosa F, Mir FF, et al. Optimization of Lipid Nanoparticle Formulations for mRNA Delivery in Vivo with Fractional Factorial and Definitive Screening Designs. *Nano Lett*. 2015; pp. 7300–7306.

7. Hui SW, Langner M, Zhao YL, Ross P, Hurley E, Chan K. The role of helper lipids in cationic liposome-mediated gene transfer. *Biophys J*. 1996; 71: 590–599.

8. Whitehead KA, Matthews J, Chang PH, Niroui F, Robert Dorkin J, Severgnini M, et al. In Vitro–In Vivo Translation of Lipid Nanoparticles for Hepatocellular siRNA Delivery. *ACS Nano*. 2012; pp. 6922–6929.

9. Paunovska K, Sago CD, Monaco CM, Hudson WH, Castro MG, Rudoltz TG, et al. A Direct Comparison of in Vitro and in Vivo Nucleic Acid Delivery Mediated by Hundreds of Nanoparticles Reveals a Weak Correlation. *Nano Lett*. 2018; pp. 2148–2157.

10. Kulkarni JA, Myhre JL, Chen S, Tam YYC, Danescu A, Richman JM, et al. Design of lipid nanoparticles for in vitro and in vivo delivery of plasmid DNA. *Nanomed: Nanotech, Biol Med*. 2017; pp. 1377–1387.

11. Farhood, H., Serbina, N., Huang, L. The role of dioleoyl phosphatidylethanolamine in cationic liposome mediated gene transfer. *Biochim Biophys- Biomemb.* 1995; 1235: 289–295.

12. Li D-W, He F-L, He J, Deng X, Liu Y-L, Liu Y-Y, et al. From 2D to 3D: The morphology, proliferation and differentiation of MC3T3-E1 on silk fibroin/chitosan matrices. *Carb Polym*. 2017; pp. 69–77.

13. Bell CC, Hendriks DFG, Moro SML, Ellis E, Walsh J, Renblom A, et al. Characterization of primary human hepatocyte spheroids as a model system for drug-induced liver injury, liver function and disease. *Sci Rep.* 2016; 6: 25187.

14. Gómez-Lechón MJ, Tolosa L, Conde I, Donato MT. Competency of different cell models to predict human hepatotoxic drugs. *Expert Opin Drug Metab Toxicol*. 2014; 10: 1553–1568.

15. Vinci M, Gowan S, Boxall F, Patterson L, Zimmermann M, Court W, et al. Advances in establishment and analysis of three-dimensional tumor spheroid-based functional assays for target validation and drug evaluation. *BMC Biology*. 2012; p. 29.

16. Edmondson R, Broglie JJ, Adcock AF, Yang L. Three-dimensional cell culture systems and their applications in drug discovery and cell-based biosensors. *Assay Drug Dev Technol.* 2014; 12: 207–218.

17. Mehta G, Hsiao AY, Ingram M, Luker GD, Takayama S. Opportunities and challenges for use of tumor spheroids as models to test drug delivery and efficacy. *J Control Release.* 2012; 164: 192–204.

18. Nunes AS, Barros AS, Costa EC, Moreira AF, Correia IJ. 3D tumor spheroids as in vitro models to mimic in vivo human solid tumors resistance to therapeutic drugs. *Biotech. Bioeng*. 2019; pp. 206–226.

19. Corning 3D Spheroid-qualified Primary Human Hepatocytes: Instruction for Primary Human Hepatocyte Spheroid Culture (Cat. No. 454552). 6 Henshaw Street Woburn, A 01801: Corning Incorporated.

20. Heger JI, Froehlich K, Pastuschek J, Schmidt A, Baer C, Mrowka R, et al. Human serum alters cell culture behavior and improves spheroid formation in comparison to fetal bovine serum. *Exp Cell Res.* 2018; 365: 57–65.

21. Mueller D, Koetemann A, Noor F. Organotypic Cultures of Hepg2 Cells for In Vitro Toxicity Studies. *J. Bioeng. Biomed Sci*. 2011; S2.

22. Wallenstein EJ, Barminko J, Schloss RS, Yarmush ML. Serum starvation improves transient transfection efficiency in differentiating embryonic stem cells. *Biotechnol Prog*. 2010; 26: 1714–1723.

23. Zanoni M, Piccinini F, Arienti C, Zamagni A, Santi S, Polico R, et al. 3D tumor spheroid models for in vitro therapeutic screening: a systematic approach to enhance the biological relevance of data obtained. *Sci. Rep.* 2016; 6: 19103.

24. Hendriks DFG, Fredriksson Puigvert L, Messner S, Mortiz W, Ingelman-Sundberg M. Hepatic 3D spheroid models for the detection and study of compounds with cholestatic liability. *Sci Rep.* 2016; 6: 35434.

25. Pramfalk C, Larsson L, Härdfeldt J, Eriksson M, Parini P. Culturing of HepG2 cells with human serum improve their functionality and suitability in studies of lipid metabolism. *Biochim Biophys Acta*. 2016; 1861: 51–59.

26. Shi J, Wang X, Lyu L, Jiang H, Zhu H-J. Comparison of Protein Expressions between Human Livers and the Hepatic Cell Lines HepG2, Hep3B and Huh7 using SWATH and MRM-HR Proteomics: Focusing on Drug-Metabolizing Enzymes. *Drug Metab Pharmacokinet.* 2018; 33: 133.

27. Qiu G-H, Xie X, Xu F, Shi X, Wang Y, Deng L. Distinctive pharmacological differences between liver cancer cell lines HepG2 and Hep3B. *Cytotechnology.* 2015; 67: 1.

28. Godoy P, Hewitt NJ, Albrecht U, Andersen ME, Ansari N, Bhattacharya S, et al. Recent advances in 2D and 3D in vitro systems using primary hepatocytes, alternative hepatocyte sources and non-parenchymal liver cells and their use in investigating mechanisms of hepatotoxicity, cell signaling and ADME. *Arch Toxicol.* 2013; 87: 1315.

29. Xue HY, Guo P, Wen W-C, Wong HL. Lipid-Based Nanocarriers for RNA Delivery. *Curr Pharm Des.* 2015; 21: 3140.

30. Kurzchalia TV, Dupree P, Parton RG, Kellner R, Virta H, Lehnert M, et al. VIP21, a 21-kD membrane protein is an integral component of trans-Golgi-network-derived transport vesicles. *J Cell Biol.* 1992; 118: 1003–1014.

31. Xue HY, Narvikar M, Zhao J-B, Wong HL. Lipid Encapsulation of Cationic Polymers in Hybrid Nanocarriers Reduces Their Non-Specific Toxicity to Breast Epithelial Cells. *Pharm Res*. 2013; 30: 572–583.

32. Whitehead KA, Dorkin JR, Vegas AJ, Chang PH, Veiseh O, Matthews J, et al. Degradable lipid nanoparticles with predictable in vivo siRNA delivery activity. *Nat Commun.* 2014; 5: 4277.

Curriculum Vitae

Education:

Johns Hopkins University *Aug. 2018 – Dec. 2019*

- Anticipated Graduation: December 2019
- Area of Study: Chemical and Biomolecular Engineering, Master of Science in Engineering

Pacific Lutheran University *Aug. 2014 – May 2018*

- Graduated May 2018, *cum laude*
- Area of Study: Chemistry, Bachelor of Science, Biology, Bachelor of Science
- Study Away Spring, 2017: University of Namibia

Graduate Research Experience:

INBT Coop Internship – Johns Hopkins University and AstraZeneca *Jan. 2019 – July 2019*

- Research Mentors: Dr. J Luis Santos (AZ), Dr. G Patrick Hussmann (AZ), Dr. Jordan J Green (JHU)
- Research Focus: Implementing in vitro screening tools for evaluating novel mRNA-nanoparticulate formulations
- Developed a thorough protocol for the culture of immortalized hepatocellular lines as 3D spheroids
- Synthesized nanoparticle formulations for drug delivery via microfluidic technology
- Characterized nanoparticle formulations via Reverse-Phase Liquid Chromatography, Ribogreen fluorescence assay, and with a Malvern Zeta-Sizer

- Designed and performed experiments to examine a possible in vitro in vivo correlation: including lipid nanoparticle transfection of cells, eGFP monitoring, Steady-Glo and Cell-Titer Glo luminescence assays

Johns Hopkins Center for a Livable Future and World Wildlife Fund *Oct 2018 – Jan 2019*

- Research Mentors: Dr. Roni Neff, Dr. Jillian Fry, Dr. Dave Love, Erin Biehl
- Research Focus: Addressing seafood waste by promoting frozen purchasing
- Identified and contacted retail seafood organizations in the Baltimore, Maryland area to interview
- Conducted qualitative interviews with retail seafood staff in order to understand seafood sustainability
- Transcribed qualitative interviews and identified important preliminary findings
- Reported interview findings to principle investigators for manuscript compilation

Undergraduate Research Experience:

Natural Sciences Summer 2017 Undergraduate Research Program *June 2017 – Aug. 2017*

- Research Mentor: Dr. Andrea M. Munro
- Research Focus: Synthesis of Mn:ZnSe/ZnS nanocrystals and ligand exchange
- Synthesized CdSe and ZnSe nanocrystals using air-free techniques
- Used SILAR techniques to grow spherical shells on CdSe nanocrystals
- Characterized products via FTIR, NMR, and XRD
- Facilitated ligand exchange, characterized with FTIR and NMR
- Continued research in Dr. Munro's lab throughout the academic year, ending in May 2018

Organic Special Projects Laboratory *Feb. 2016 – May 2016*

- Research Mentor: Dr. Neal A. Yakelis
- Research Focus: Development of aryldiborate weakly coordinating dianions
- Attempted synthesis via Grignard attack in an air-free environment
- Characterized products and quantified relative yield via GC-MS

Other Relevant Laboratory Experience:

Determination of concentration with Inductively Coupled Plasma Atomic Emission Spectroscopy

Spectrophotometric analysis via UV-Visible Spectroscopy

Super-critical fluid extraction

Determination of unknown mixture with Thin Layer Chromatography

Green organic synthesis via sonication

Microwave synthesis

Presentations:

Spring 2018 Biology Capstone Symposium *May 2018*

- Oral Presentation: Kisspeptin as a modulator of sexual behavior in rodents

2018 Chemistry Capstone Symposium *May 2018*

- Oral Presentation: Improving luminescent solar concentrator efficiency using doped nanocrystals and ligand exchange

26th Annual Murdock College Science Research Conference *Nov. 2017*

- Poster Presentation: Improving luminescent solar concentrator efficiency using doped nanocrystals and ligand exchange

Natural Sciences Summer Undergraduate Research Presentations *Sept. 2017*

- Oral Presentation: Improving luminescent solar concentrator efficiency using doped nanocrystals and ligand exchange

Murdock Collaborative Research Alliance Collaborative Meeting *June 2017*

- Oral Presentation: Nanocrystals: Exploring diffusion doping, shells, and ligand exchange

PLU Natural Sciences Academic Festival Poster Session *May 2016*

- Poster Presentation: Development of aryldiborate weakly coordinating dianions

ACS Puget Sound Undergraduate Research Symposium *Apr. 2016*

- Poster Presentation: Development of aryldiborate weakly coordinating dianions

Clinical Shadowing Experience

Medstar Promptcare at Alexandria *May 2019 – July 2019*

- Shadowed Dr. E. Kate Snodgrass
- Observed diagnosis and treatment of bacterial and viral infections, injuries, and long-term health concerns

Vic's Family Pharmacy *Aug. 2016*

- Shadowed Dr. Victor Allen
- Observed retail, long-term care, and compound pharmacy techniques
- Earned "HIPPA" and "Fraud, Waste, and Abuse" Certifications

Lovelace and Kido Dental *Jan. 2014 – May 2014*

- Shadowed Dr. Lori Lovelace and Dr. Scott Kido
- Observed routine and emergency dental procedures

Volunteer Experience

Johns Hopkins Children's Hospital	*Sept. 2019 – Present*
Maryland SPCA	*Oct. 2018 – Present*
Hope Village Orphanage	*Jan. 2017 – May 2017*
Sherman Elementary School	*June 2011 – Aug. 2014*
Lighthouse Rescue Mission	*Aug. 2013 – May 2014*

Honors and Awards:

Pacific Lutheran University -- Ramstad Scholar (2017)

Pacific Lutheran University -- Dean's List (Aug. 2014 – May 2018)

Idaho High School State Athletics Association -- Track and Field State Qualifier (2014)

Skyview High School -- Student Leadership Award (2014)

Skyview High School -- Junior Varsity Women's Soccer Captain (2011-2013)